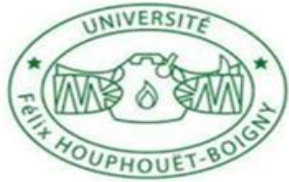


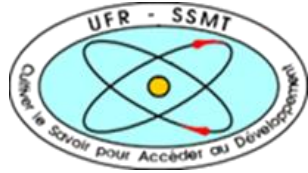
MINISTERE DE L'ENSEIGNEMENT  
SUPERIEUR ET DE LA  
RECHERCHE SCIENTIFIQUE  
Felix Houphouet-Boigny University



STEEL INSTITUTE OF RWTH AACHEN  
UNIVERSITY



UNITE DE FORMATION ET DE  
RECHERCHE SCIENCES DES  
STRUCTURES DE LA MATIERE  
ET DE TECHNOLOGIE



No : 826



SPONSORED BY THE

**INTERNATIONAL MASTER PROGRAM  
IN RENEWABLE ENERGY AND GREEN HYDROGEN  
SPECIALITY: GREEN HYDROGEN PRODUCTION AND  
TECHNOLOGY TRACT  
MASTER THESIS**

Subject/Topic:

**Microstructural Characterization and Study of Hydrogen  
Embrittlement in Duplex Stainless Steels**

Presented on the 23<sup>rd</sup> of September by:

**ADEWUMI, ABAYOMI OLUMUYIWA**

**President of the Jury:**

Prof. KOUADIO Kouassi Yves

**Examiner:**

Dr. (MC) ESSY Kouadio Fodjo

**Major Supervisor**

Dr. Eric Kessein Tillous

**Co-Supervisor**

Univ. Prof. Dr.-Ing. Ulrich Krupp

**Co-Supervisor**

Nima Babaei, M.Sc.

Academic year 2024-2025

## **Dedication**

To my dearest family,  
this work is a reflection of your endless love, sacrifice, and encouragement. At every step of this journey, your unwavering support has been my strength, and your faith in me has been my greatest source of motivation. Every achievement I celebrate today is rooted in the values, patience, and guidance you have given me.

With the deepest gratitude and all my love, I dedicate this work to you, a humble token of appreciation for all that you mean to me....

ADEWUMI, Abayomi Olumuyiwa

## Acknowledgments

I wish to express my deepest gratitude to all those whose support and contributions have made this academic journey possible.

First, I am sincerely grateful for the financial support provided by the German Federal Ministry of Education and Research (BMBF) under the auspices of the West African Science Service Center for Climate Change and Adapted Land Use (WASCAL), through the international Master Program in Energy and Green Hydrogen. Without this support, this work would not have been possible.

My appreciation goes to the University Felix Houphouet Boigny (Prof. Ballo Zie, President), University Abdou Moumouni (Prof. Adamou Rabani, Rector), and the Directors of the Graduate Schools of Pan-African Studies in Niger and Cote d'Ivoire (Prof. Rabani Adamou and Prof. Kouassi Edouard).

I also extend my thanks to Dr. Kessein Eric Tillous, my supervisor and Coordinator of the Hydrogen Program at GSP, Dr. Fassinou Wanignon Ferdinand, the Scientific Coordinator also for their tireless guidance and leadership throughout the program.

I am very grateful to the RWTH Aachen University, the Rector; Prof. Ulrich Rudiger, to my supervisor at the Institut für Eisenhüttenkunde (IEHK), Prof. Dr.-Ing. Ulrich Krupp, for giving me the chance to do my research internship in Germany. My special appreciation goes to the co-supervisor, Mr Nima Babaei, for his mentorship, insights, and helpful criticism which substantially enhanced this project.

My gratitude also goes to the members of the jury, which includes the esteemed President; Prof. KOUADIO Kouassi Yves and the Examiner; Dr. (MC) ESSY Kouadio Fodjo of the University Felix Houphouet Boigny, for their careful review and comments on this work.

I would like to extend my appreciation to the entire WASCAL family and my fellow classmates across Togo, Niger, Cote d'Ivoire, and Germany, with whom I shared four semesters of training. This trip was successful and unforgettable because of your cooperation and support.

Finally, I am deeply indebted to my family. To my late Father, Pastor Duro Adewumi, whose encouragement and sacrifices laid the foundation for my achievements. To my mother, Chief Mrs. Victoria Adewumi, my backbone and source of strength. To my beloved wife, Mrs. Opeyemi Adewumi, who held the home together during my absence, my emotional support, and to my children, Oluwasanmi, Oluwatofiyin, and Oluwajomiloju, for being my greatest motivation. My gratitude also goes to my siblings, Mrs Boyejo Olubusayo and Mr. Olumide Adewumi, and to my in-laws, Prof. F.A. Adekayode and Mrs. Adekayode, for their support. In

particular, I am thankful to Prof F.A Adekayode, who went beyond family duty to assist with the vetting and correction of this thesis, your input added immense value to my work. To the Segbe Family, in particular Mama Segbe and Madam Sefako Segbe, for your love, hospitality and care during my time in Togo. I am grateful.

To everyone, this accomplishment is a direct result of your unshakeable faith in me. I am eternally indebted and immensely thankful.

## Abstract

Hydrogen embrittlement (HE) remains a critical challenge in the deployment of duplex stainless steels (DSS) for energy, maritime and chemical processing applications. The duplex stainless Steel having a unique dual-phase microstructure of austenite and ferrite, which offers high strength and corrosion resistance, thereby making it a suitable candidate for use in harsh environments. However, exposure to environments with a high hydrogen content can severely reduce its mechanical performance, leading to premature and often catastrophic failure.

This study examines how hydrogen charging affects the tensile behaviour and fracture properties of DSS using the slow strain rate testing (SSRT), the In-situ SSRT under electrochemical hydrogen charging, and the thermal desorption analysis (TDA). Samples were examined for microstructural characteristics using the scanning electron microscope (SEM) in order to evaluate the phase balance and fracture modes. It was discovered that with hydrogen charging, there was a noticeable loss in strength and ductility, a distinct change from ductile to brittle fracture modes, and hydrogen trapping behaviour that is associated with certain microstructural characteristics. These result offers a useful understanding into how hydrogen interacts with DSS and contribute towards developing mitigation plans for the safer and more reliable use of DSS in hydrogen service applications.

**Keywords:** Duplex stainless steel; hydrogen embrittlement; slow strain rate testing; thermal desorption analysis; scanning electron microscopy

## Résumé

La fragilisation par l'hydrogène (HE) reste un défi majeur dans le déploiement des aciers inoxydables duplex (DSS) pour les applications énergétiques, maritimes et chimiques. L'acier inoxydable duplex possède une microstructure biphasée unique composée d'austénite et de ferrite, qui lui confère une résistance élevée et une bonne résistance à la corrosion, ce qui en fait un candidat idéal pour une utilisation dans des environnements difficiles. Cependant, l'exposition à l'hydrogène peut réduire considérablement ses performances mécaniques, entraînant une défaillance prématuée et souvent catastrophique.

Cette étude examine comment le chargement en hydrogène affecte le comportement à la traction et les propriétés de fracture des aciers inoxydables duplex (DSS) en utilisant des tests à taux de déformation lente (SSRT), le SSRT in situ sous chargement électrochimique en hydrogène et l'analyse de désorption thermique (TDA). Des échantillons ont été examinés pour caractériser les propriétés microstructurelles à l'aide d'un microscope électronique à balayage (SEM) afin d'évaluer l'équilibre des phases et les modes de fracture. Il a été découvert qu'avec le chargement en hydrogène, il y avait une perte notable de résistance et de ductilité, un changement distinct de modes de fracture ductiles à fragiles, et un comportement de piégeage de l'hydrogène associé à certaines caractéristiques microstructurelles. Ces résultats offrent une compréhension utile de la façon dont l'hydrogène interagit avec les DSS et contribuent à l'élaboration de plans d'atténuation pour une utilisation plus sûre et plus fiable des DSS dans les applications de service à l'hydrogène.

**Mots clés: acier inoxydable duplex; fragilisation par l'hydrogène; essai à faible vitesse de déformation; analyse par désorption thermique; microscopie électronique à balayage**

## **List Of Tables**

Table 1.1: Chemical composition of exemplary austenitic and ferritic stainless-steel grades	9
Table 1.2: Effect of the alloying elements on phase stabilities	10
Table 1.3: Composition of the duplex stainless-steel alloys	12
Table 1.4: Mechanical properties of the duplex stainless-steel Alloys	12
Table 3.1: Chemical composition of duplex Stainless steel	35
Table 3.2: SEM Image Parameters	44
Table 3.3: Mechanical comparison In-Air versus hydrogen charged	46

## List Of Figures

Figure 1.1: Optical observation of DSS after metallographic preparation: .....	6
Figure 1.2: (a) an Optical Micrograph (b) a Scanning Electron micrograph of the as received hot rolled DSS, showing austenite and ferrite phase (Olanipekun et al., 2019).....	7
Figure 1.3: Phase diagram of duplex steel (Liao and Chumbley, 2019).....	8
Figure 1.4: The diagrammatic representation of the HELP mechanism: the presence of hydrogen encourages dislocation mobility and localises plastic deformation at the crack tip; the microcavities in this area of high hydrogen concentration and hydrostatic stress coalesce to cause the crack to propagate (Tomoki, 2019). .....	14
Figure 1.5: The diagrammatic representation of potential HEDE-producing zones (a) near the tip of the Crack; (b) a few tens of nanometres distant from the tip and (c) at grain to grain or precipitate to precipitate interfaces (Tomoki, 2019). .....	15
Figure 1.6: The AIDE mechanism is shown schematically. The two stages of embrittlement are the nucleation and growth of microcavities ahead of the crack tip and the local reduction of the material's cohesion energy, which encourages the nucleation and the emission of dislocations from the crack tip (Dwivedi and Vishwakarma, (2018)). .....	15
Figure 1.7: Hydrogen diffusion coefficient in ferrite and austenite depending on the temperature. (Klett and T. Hassel, 2020) .....	16
Figure 1.8: Changes in engineering stress–strain curve with and without in-situ electrochemical hydrogen charging at the strain rate of $3.4 \times 10^{-6} \text{ s}^{-1}$ . Source: (Pichler et al., 2023).....	18
Figure 1.9: Schematic diagram of hydrogen permeation test device. (Li et al., 2023). .....	19
Figure 1.10: Schematic diagram of Thermal Desorption Analysis (Fangnon et al., 2020). ....	20
Figure 1.11: TDA curves corresponding to measurement procedures 1,2, with the same AVC dwelling time which is 15 minutes (a) and Procedure 3, 4, with the same AVC dwelling time which is 60 mins on (b) (Fangnon et al., 2020).....	21
Figure 1.12: In-situ SSRT schematic showing loading and Hydrogen charging system. Source: (Fu et al., 2020) .....	22
Figure 2.1: Dimension of the tensile test sample .....	25
Figure 2.2: The tensile test sample, indicating the charging are .....	26
Figure 2.3: The test sample .....	26
Figure 2.4: The specimen before the grinding process .....	27
Figure 2.5: The Saphir M1 Grinding and Polishing machine .....	27
Figure 2.6: The SiC papers.....	28

Figure 2.7: During grinding procedure .....	28
Figure 2.8: An ultrasonic cleansing beaker .....	28
Figure 2.9: The dryer.....	28
Figure 2.10: Diamond suspensions .....	29
Figure 2.11: Polishing procedures.....	29
Figure 2.12: Specimen after polishing .....	29
Figure 2.13: Etching procedure inside the solution.....	29
Figure 2.14: The test sample with the non-reactive insulating tapes .....	30
Figure 2.15: Material testing equipment (a) Before set-up (b) During SSRT setup .....	31
Figure 2.16: Non-reactive tape .....	31
Figure 2.17: The In-situ SSRT Setup .....	31
Figure 2.18: Complete in-situ SSRT setup.....	32
Figure 2.19: BRUKER IR07 Analyzer .....	33
Figure 2.20: Mettler Toledo ME204 analytical balance .....	33
Figure 3.1: Microstructural analysis at 500X magnification.....	35
Figure 3.2: Microstructural analysis at 1000X magnification.....	35
Figure 3.3: Microstructure at 1250 °C, 90 mins 100X magnification .....	36
Figure 3.4: Stress-length change curve of DSS in-Air.....	37
Figure 3.5: Stress-strain curve of DSS in-Air .....	37
Figure 3.6: Stress-length change curve under hydrogen charging .....	38
Figure 3.7: Stress-Strain Curve under Hydrogen Charging .....	39
Figure 3.8: TDA desorption over Time.....	40
Figure 3.9: TDA desorption curve of DSS as temperature rises .....	41
Figure 3.10: Figures a, b and c indicate the In Air SEM imagery while Figures d, e and f indicates under Hydrogen Charging SEM imagery. .....	43
Figure 3.11: Combined stress-length change curves.....	45
Figure 3.12:Combined stress-strain curves .....	45

## Acronyms And Abbreviations

Abbreviations	Description
ASTM:	American Society for Testing and Materials
CSR:	Corporate Social Responsibility
DSS:	Duplex Stainless Steel
H <sub>2</sub> SO <sub>4</sub> :	Sulfuric Acid
H <sub>2</sub> :	Hydrogen
HEDE:	Hydrogen-Enhanced Decohesion
HELP:	Hydrogen-Enhanced Localized Plasticity
IEHK:	Institut für Eisenhüttenkunde (Institute of Ferrous Metallurgy)
MEP:	Mechanical, Electrical, and Plumbing
MPa:	Megapascal
MS:	Mild Steel
OM:	Optical Microscopy
ppm:	Parts Per Million
RCDPP:	Research Centre for Digital Photonic Production
SEM:	Scanning Electron Microscopy/ Microscope
SSRT:	Slow Strain Rate Test
TDA:	Thermal Desorption Analysis
UTS:	Ultimate Tensile Strength
ksi	Kilopounds per square inch
AVC	Absolute Vacuum Capillary
RDS	Rediffusion Simulation/Rediffusion Signal
CRAs	Corrosion Resistant Alloys

## List of Units and Symbols

Units	Nomenclature
$^{\circ}\text{C}$	Degrees Celsius (Temperature)
<b>MPa</b>	Megapascal, Unit of stress (e.g., yield strength, tensile strength)
<b>s</b>	Seconds (time, time of failure)
$s^{-1}$	Per second, reciprocal seconds (strain rate)
<b>K/s</b>	Kelvin per second (heating rate in TDA)
<b>ppm</b>	Parts per million (hydrogen concentration)
<b>wt.%</b>	Weight percent (Chemical composition)
<b>%</b>	Percentage (elongation, Phase content, strain, reduction of area)

## Symbols

<b><math>\sigma</math></b>	Stress ( $\sigma_y$ = Yield strength, $\sigma_u$ = Ultimate tensile strength)
<b><math>\epsilon</math></b>	Strain (uniform strain, elongation at fracture)
<b><math>\gamma</math></b>	Austenite phase
<b><math>\alpha</math></b>	Ferrite phase

## Table of Contents

Dedication .....	i
Acknowledgments .....	ii
Abstract .....	iv
List Of Tables .....	vi
List Of Figures .....	vii
Acronyms And Abbreviations.....	ix
List of Units and Symbols .....	x
Table of Contents .....	xi
General Introduction .....	2
Research Question.....	3
Objectives of the Study .....	3
<b>1. LITERATURE REVIEW.....</b>	<b>5</b>
1.1 What are Duplex Steels .....	5
1.2 Historical Development of Duplex Stainless Steels.....	6
1.3 Microstructure and Phases .....	7
1.4 Alloying Elements and Range of Usage in Duplex Stainless Steels.....	8
1.4.1 Effect of Alloying Elements on Phase Stabilities .....	9
1.5 Classification of Duplex Stainless Steels DSS .....	10
1.5.1 Range of usage .....	11
1.6 Mechanical and Corrosion properties of duplex stainless steel .....	11
1.7 Microstructural challenges and processing .....	12
1.8 Hydrogen Embrittlement in DSS .....	13
1.8.1 Mechanism of Hydrogen Embrittlement in DSS .....	13
1.8.2 Influence of Microstructure:.....	16
1.8.3 Testing and Assessment of Hydrogen Embrittlement in DSS: .....	17
1.8.4 Mitigation Approaches: .....	22

<b>2. MATERIAL AND METHODS.....</b>	<b>25</b>
2.1 Materials and Chemical Composition .....	25
2.2 Metallographic Preparation .....	26
2.3 Electrochemical Hydrogen Charging .....	30
2.4 The Slow Strain Rate Test.....	30
2.5 Hydrogen Analysis (TDA) .....	32
2.6 Data Processing and Analysis .....	33
<b>3. RESULTS AND DISCUSSION.....</b>	<b>35</b>
3.1 Chemical Composition.....	35
3.2 Microstructural Analysis (Metallography).....	35
3.3 Mechanical Testing .....	36
3.3.1 SSRT in Air (without hydrogen charging) .....	36
3.3.2 In-Situ SSRT under Hydrogen Charging .....	38
3.4 Thermal Desorption Analysis (TDA).....	39
3.5 Fractographic Observation .....	42
3.6 Discussion .....	44
3.7 Partial Conclusion .....	47
<b>GENERAL CONCLUSION .....</b>	<b>49</b>
<b>PERSPECTIVE.....</b>	<b>50</b>
<b>REFERENCES .....</b>	Error! Bookmark not defined.

# **GENERAL INTRODUCTION**

## General Introduction

The global energy landscape is undergoing a rapid transformation, which is driven by the urgent need to reduce greenhouse gas emissions and move towards cleaner and more appropriate technologies. Hydrogen has shown to be a promising energy carrier, also as a mean of achieving decarbonization in diverse sectors such as the power generation, transportation, and other heavy industries. But as the adoption of hydrogen grows, so does the difficulty of ensuring the safety and the reliability of the infrastructure that is required for its storage, transportation and delivery to the utility.

Duplex stainless steels (DSS) are highly desirable for their outstanding combination of mechanical strength, corrosion resistance, and affordability. These qualities make them suitable for use in pipelines, pressure vessels, and other hydrogen service components. However, the hydrogen embrittlement (HE) is a serious flaw that undermines their long-term performance. Hydrogen can hasten failure, decrease fracture toughness, and decreases ductility when it penetrates the metal lattice, often without any visible warning signs. Therefore, in demanding applications, where structural failure might have serious safety and economic consequences, this risk is magnified.

As Africa pushes towards adopting green hydrogen as part of its renewable energy transition program, it is imperative to consider how dependable the materials to be used are, especially in storage, production and in the transportation. If HE is not properly understood and controlled, this could lead to unexpected failures, safety hazards and high maintenance cost which may impede or halt the ambitions for green hydrogen in Africa.

In order to address this challenge, a variety of sophisticated experimental techniques are used in this study; the slow strain rate testing (SSRT) to evaluate the mechanical response of DSS under controlled loading conditions; the in-situ SSRT under electrochemical hydrogen charging to simulate real-time exposure to hydrogen while under stress; the thermal desorption analysis (TDA) to measure the amount of hydrogen content present, and to locate trapping sites within the material; and the use of Optical microscopy and scanning electron microscopy (SEM) for microstructural and fractographic analysis, which allows for direct observation of phase distribution and fracture features.

By combining mechanical testing, hydrogen quantification, and microstructure characterization, this work offers a comprehensive understanding of hydrogen embrittlement in DSS. The result will help ensure the safe deployment of DSS in hydrogen related infrastructure and guide with the material selection, processing methods, and maintenance strategies in the

developing hydrogen economy and the knowledge also benefiting Africa.

## **Research Question**

How does the microstructure and phase balance of duplex stainless-steel influences its mechanical performance and its susceptibility to hydrogen embrittlement?

## **Objectives of the Study**

The overall aim of this research is to investigate the duplex stainless steel (DSS) to hydrogen embrittlement and to connect its mechanical and microstructural behaviour to hydrogen interaction processes. In order to do this, the study sets out the objectives.

The study starts by using duplex stainless steel (DSS) standard composition, with its phase balance being verified through optical microscopy. Then the mechanical properties are evaluated by conducting the slow strain rate testing (SSRT) in both air and under in-situ hydrogen charging conditions. The hydrogen retention content in the steel is then measured using the thermal desorption analysis (TDA). Finally, the relationship between the phase distribution, strength, ductility and fracture behaviour is explored using the scanning electron microscopy (SEM) which is used for detailed fractography analysis. This approach helps to clarify the role of phase balance in hydrogen embrittlement resistance.

# **CHAPTER I:**

## **LITERATURE REVIEW**

## 1. LITERATURE REVIEW

### Introduction

Duplex Stainless Steels (DSS) have gained a lot of prominence in industrial applications because of their exceptional combination of mechanical strength, corrosion resistance, and cost-effectiveness. Unlike conventional single-phase stainless steels, DSS are characterized by a biphasic microstructure composed of approximately equal volume fractions of ferrite and austenite phases, which is typically within the range of 40-60% each. Particularly in situations with high chloride content, this microstructure balance provides enhanced resistance to pitting, crevice corrosion, and stress corrosion cracking. (Gunn, 1997)

Over the years, developments in alloying designs, thermomechanical processing, and welding methods have enhanced the versatility of DSS, thereby making them appropriate for crucial applications in oil and gas, marine, chemical, and other increasing hydrogen infrastructure. However, the addition of DSS into systems using hydrogen has brought an attention to a significant weakness: the hydrogen embrittlement, which may cause premature material failure (Francis and Byrne, 2021). It is crucial to fully understand how microstructure, alloy composition, and external factors influence DSS performance in hydrogen environments.

This literature review explores the historical evolution, microstructure, and primary performance concerns of DSS with a specific focus on how they behave under hydrogen related stress and the testing techniques that are used to assess it. It also examines the recent studies on hydrogen embrittlement testing methods and how they advance our understanding of failure processes in DSS. This review aims to establish the framework for evaluating their long-term feasibility in hydrogen infrastructure.

#### 1.1 What are Duplex Steels

Duplex Stainless Steels (DSS) represents a class of corrosion-resistant alloys with a distinctive two-phase microstructure which consist of both ferrite ( $\alpha$ ) and austenite ( $\gamma$ ) in nearly equal proportions (Gunn, 1997; Liao and Chumbley, 2019). This combination results in a material that merges the best properties of both phases: the high strength of ferrite and the ductility and the corrosion resistance of austenite. This balanced microstructure imparts a unique combination of high strength, toughness and excellent corrosion resistance, making DSS highly suitable for demanding applications in industries such as oil and gas, chemical processing and marine engineering (Gunn, 1997).

Ferrite, with its Body-Centred Cubic (BCC) structure, contributes to high yield strength, resistance to stress corrosion cracking (SCC), and rapid hydrogen diffusion. However, it is typically less ductile than austenite. (Gunn, 1997; Han *et al.*, 2023). Austenite, with a Face-Centred Cubic (FCC) structure, offers high ductility, toughness, and superior general corrosion resistance (Knyazeva and Pohl, 2013). It has a greater capacity to absorb hydrogen but allows slower hydrogen diffusion (Francis and Byrne, 2021).

The formation of this dual-phase structure has a significant impact on the alloy composition and cooling conditions. Usually, DSS solidifies first as ferrite, then austenite forms from ferrite during subsequent cooling. The ideal microstructural balance is about 50:50, which enhances both mechanical and corrosion properties.

Figure 1.1, the microstructure of both a hot-rolled and annealed (HRA) sample and a cold-rolled and annealed (CRA) sample are shown. The green and red colour corresponds to the austenite and ferrite phases respectively, while the blue and black lines demonstrates low angle and high angle boundaries (Han *et al.*, 2017).

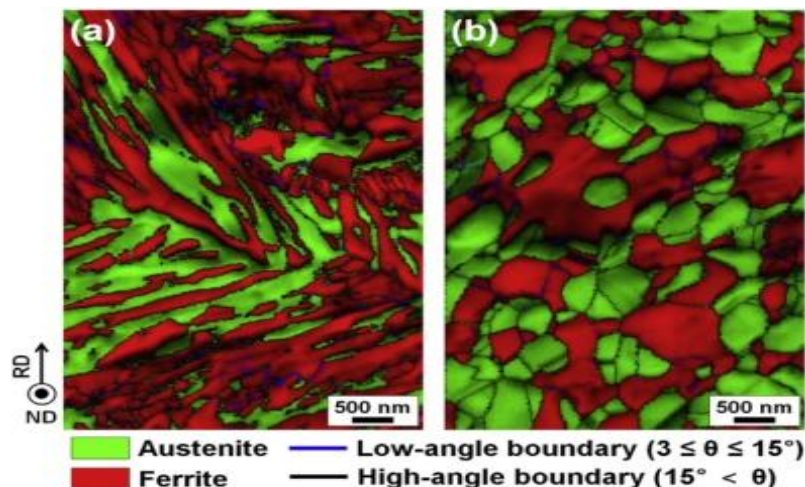


Figure 1.1: Optical observation of DSS after metallographic preparation:

(a) the hot-rolled and annealed (HRA) specimen and (b) the cold-rolled and annealed (CRA) specimen (Han *et al.*, 2017).

## 1.2 Historical Development of Duplex Stainless Steels

The history of DSS dates back to the 1930s, with early developments led by Swedish manufacturers. However, practical use was limited until the 1970s due to challenges in metallurgy and fabrication. The turning point came with the introduction of the AOD (Argon

Oxygen Decarburisation) and VOD (Vacuum Oxygen Decarburisation) refining processes, which enabled better control of nitrogen and carbon content. These advancements allowed the production of grades like UNS S31803, which had balance corrosion resistance and improved weldability (Gunn, 1997; Francis and Byrne, 2021).

### 1.3 Microstructure and Phases

The characteristics feature of DSS is their biphasic structure. The ferrite phase is known to offer high strength resistance to stress corrosion cracking, while austenite improves the material's overall toughness and corrosion resistance. The typical microstructure after proper heat treatment shows elongated austenite islands embedded in a ferritic matrix (Knyazeva and Pohl, 2013). Figure 1.2 shows the schematic representation of nanoindentation head (Olanipekun *et al.*, 2019). The nanoindentation head is a component in the nanoindentation system, used to measure the mechanical properties of materials at the nanoscale.

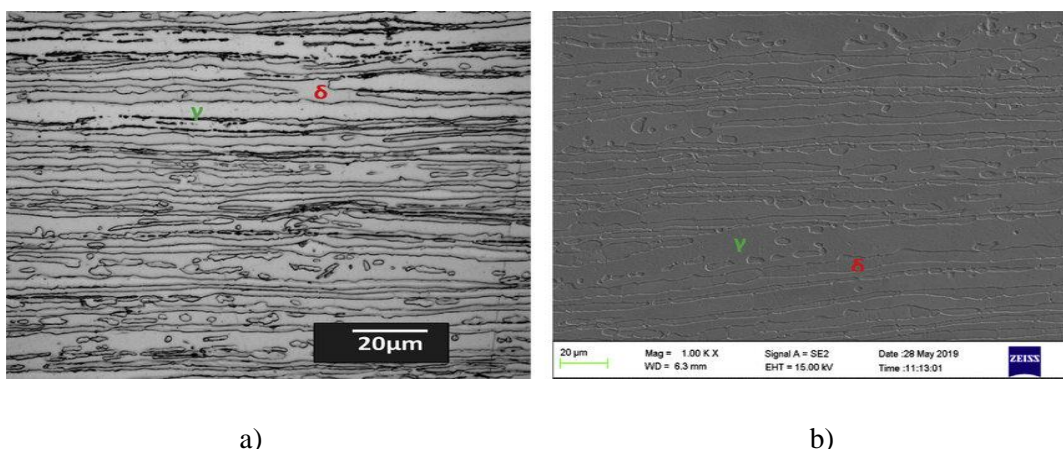


Figure 1.2: (a) an Optical Micrograph (b) a Scanning Electron micrograph of the as received hot rolled DSS, showing austenite and ferrite phase (Olanipekun *et al.*, 2019).

During casting, DSS solidifies as ferrite and when it cools, it partially changes to austenite. Heat treatment at around 1050-1100 °C followed by rapid quenching ensures a balanced microstructure and reduces the production of dangerous intermetallic phases like sigma ( $\sigma$ ) and chi ( $\chi$ ) (Gunn, 1997). According to Knyazeva and Pohl (Knyazeva and Pohl, 2013), the phase balance greatly affect the mechanical characteristics and corrosion resistance.

Figure 1.3 is showing the phase diagram of duplex stainless steels (DSS) involves a distinct transformation from fully liquid metal to a dual-phase solid microstructure of ferrite and austenite. This process is governed by the alloy composition, thermodynamic phase equilibrium.

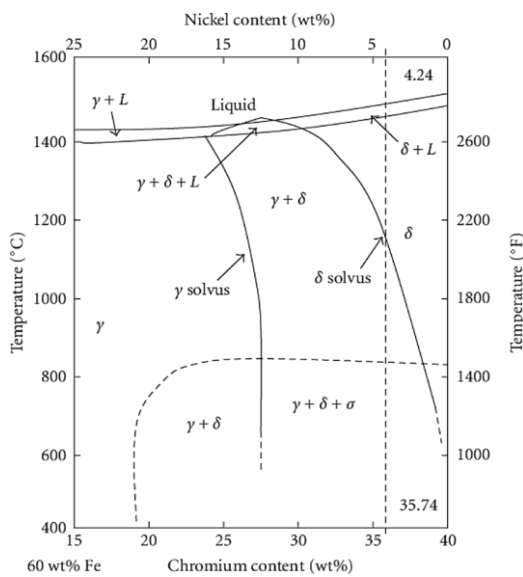


Figure 1.3: Phase diagram of duplex steel (Liao and Chumbley, 2019)

A typical solidification of DSS begins with the nucleation of ferrite from the liquid phase at the liquidus temperature. As cooling continues, austenite precipitates from ferrite through a solid-state transformation. The final microstructure consists of a near equal distribution of ferrite and austenite phases.

## 1.4 Alloying Elements and Range of Usage in Duplex Stainless Steels

The performance of duplex stainless steels (DSS) is heavily influenced by the selection and balance of alloying elements. The key alloying elements are chromium (Cr), nickel (Ni), molybdenum (Mo), nitrogen (N) and then in some cases copper (Cu) or tungsten (W) contributes to the steel's corrosion resistances, mechanical properties and phase stability.

- Chromium is the most important element for corrosion resistance, which is present in DSS grades containing 21-26 wt.% Cr. This forms a stable passive oxide film on the surface.
- Nickel is added to stabilize the austenite phase, usually in the range of 4-8 wt.%, while molybdenum improves resistance to pitting and crevice corrosion in chloride-rich environments (Gunn, 1997).
- Nitrogen as two functions; It improves pitting resistance (i.e. significantly contributes to Pitting Resistance Equivalent Number PREN) and stabilizing austenite, reducing the need for higher nickel concentration.
- Manganese may be present as a partial substitute for nickel in some lean duplex grades, but excessive Mn may negatively affect corrosion resistance. Other elements like tungsten (in

super and hyper duplex steels) and copper (to improve sulphuric acid resistance) are selectively added based on application requirements (Gunn, 1997; Han *et al.*, 2023).

A standardized duplex stainless steel such as UNS S32205 contains the following composition: it includes approximately 22-23% chromium, nickel content ranges from 4.5 to 6.5%, molybdenum at about 3 to 3.5% and Nitrogen from 0.14 to 0.20%.

Further explanation on how an Austenite-Ferrite balance is achieved can be understood on comparing the composition of two familiar steels austenitic 304, (1.4301), and ferritic 430, (1.4016). Table 1.1 indicates the chemical composition of austenitic and ferritic stainless-steel grades.

*Table 1.1: Chemical composition of exemplary austenitic and ferritic stainless-steel grades*

Structure	Grade	EN No	C	Si	Mn	P	S	N	Cr	Ni	Mo
Ferritic	430	1.4016	0.08	1.00	1.00	0.040	0.015	-	16.0/18.0	-	-
Austenitic	304	1.4301	0.07	1.00	2.00	0.045	0.015	0.11	17.5/19.5	8.0/10.5	-

The important elements in a stainless steel can be classified into ferrite stabilizers which include chromium (Cr), silicon (Si), molybdenum (Mo), tungsten (W), titanium (Ti), niobium (Nb) and the austenite stabilizers which include carbon (C), nickel (Ni), manganese (Mn), nitrogen (N), copper (Cu).

The Chemical composition of Grade 430 stainless steel is dominated by ferrite stabilizing elements, resulting to ferritic microstructure. Grade 304 becomes austenitic through the use of 8% Nickel. To achieve a balanced duplex microstructure, comprising about 50% ferrite and 50% austenite, there has to be a balance between the ferrite and austenite stabilizing alloying elements. Further reading will show us some typical composition of duplex stainless steels. (BSSA, 2025)

#### **1.4.1 Effect of Alloying Elements on Phase Stabilities**

The phase stabilities in DSS are carefully engineered by adjusting the alloying elements. These elements shift the ferrite/austenite fraction, influence the solidification pathway, and the impact corrosion resistance (Gunn, 1997; Han *et al.*, 2023). Table 1.2 explains the effect of alloying elements on phase stabilities.

Table 1.2:Effect of the alloying elements on phase stabilities

Element	Function in DSS microstructure
Cr	It stabilizes ferrite, It increases general and pitting corrosion resistance.
Ni	It stabilizes austenite, Improves ductility and weldability
Mo	It supports ferrite formation, It enhances resistance to pitting and crevice corrosion.
N	Strong austenite stabilizer; raises strength and pitting resistance
Mn	It promotes austenite, Sometimes replaces Ni in lean grades
W	It is used in Super duplex to improve pitting resistance
Cu	Enhances corrosion resistance in reducing acids
C	Kept low to avoid sensitization and intergranular corrosion

## 1.5 Classification of Duplex Stainless Steels DSS

DSS are broadly classified into four categories based on their alloy content and corrosion resistance:

1. Lean Duplex (example S32101): Lower Mo and Ni, Cost-effective, used in mild environments.
2. Standard Duplex (example S31803/S32205): Having a balanced corrosion and mechanical properties.
3. Super Duplex (example S32750): Has high PREN, excellent corrosion resistance in harsh environment.
4. Hyper Duplex: Designed for the most extreme circumstances, High alloy content and PREN (>45), (Gunn, 1997).

Each category is chosen based on application requirements, financial factor, and service environment.

### 1.5.1 Range of usage

The basic idea of duplex is to produce a chemical composition leading to an approximately equal fraction of ferrite and austenite. The range of applications for DSS stems directly from these properties. Lean duplex steels are used in structural and architectural components, while standard grades are widely used in, Oil and gas pipelines, desalination equipment, heat exchangers, pressure valves and marine hardware, respectively.

Super duplex grades (for example, UNS S32750) are commonly deployed in offshore platforms, deep-sea valves and sour gas systems due to their exceptional resistance to pitting, crevice corrosion, and stress corrosion cracking (Gunn, 1997; Han *et al.*, 2023).

The Super duplex Steels hereby produces the following advantages:

- a. Higher strength: the range of 0.2% Proof Stress (stress at which a material undergoes a specified small amount of permanent deformation) for the current duplex grades is from 400-500MPa. This can lead to reduced section thickness and therefore to reduced weight. It could be advantageous in areas such as pressure vessels and storage tanks and also in structural applications e.g. bridges.
- b. Good weldability in thick sections
- c. Good toughness, much better than ferritic steel grades in particular at low temperature, typically down to -50 °C, stretching to -80 °C.
- d. Resistance to stress corrosion cracking: it is advantageous in swimming pool structures, hot water tanks, process plant and brewing tanks (BSSA, 2025).

### 1.6 Mechanical and Corrosion properties of duplex stainless steel

Duplex stainless steel possesses superior mechanical properties compared to austenitic stainless steels. Their yield strength is typically twice as high while maintaining comparable ductility. This makes DSS suitable for pressure vessels and load bearing components (Gunn, 1997). Corrosion resistance is among the most celebrated attributes of DSS. Due to the synergy between ferrite and austenite, DSS resist localized corrosion phenomena such as pitting, crevice corrosion, and chloride stress corrosion cracking (CSCC). The pitting resistance equivalent number (PREN) is used to quantify resistance to pitting:

$$\text{PREN} = \% \text{Cr} + 3.3 \times \% \text{Mo} + 16 \times \% \text{N}$$

Standard DSS have PREN values around 35-40, while super duplex grades exceed 40, offering superior performance in seawater and sour service applications. (Francis and Byrne, 2021).

Table 1.3 indicates the five duplex stainless steels spanning a wide range of alloying levels and thus corrosion resistance (Rachel *et al.*, 2013).

Table 1.4 also describes the mechanical properties of the duplex stainless-steel alloys.

*Table 1.3:Composition of the duplex stainless-steel alloys*

UNS	EN	Cr	Ni	Mo	Mn	N	PREN
S32101	1.4162	21.5	1.5	0.3	5	0.22	26.0
S32304	1.4362	23	4.8	0.3	1	0.1	25.6
S82441	1.4662	24	3.6	1.6	3	0.27	33.6
S32205	1.4462	22	5.7	3.1	1	0.17	35.0
S32750	1.4410	25	7	4	1	0.27	42.5

*Table 1.4:Mechanical properties of the duplex stainless-steel Alloys*

(Catherine, Houska, C.S.I., 2015)

UNS	EN	Tensile strength MPa (ksi)	Min. yield strength MPa (ksi)
S32101	1.4162	650 (94)	450 (65)
S32304	1.4362	600 (87)	400 (58)
S32003	1.4062	655 (95)	450 (65)
S32205	1.4462	655 (95)	450 (65)

## 1.7 Microstructural challenges and processing

Despite their advantages, DSS can experience embrittlement due to the formation of intermetallic phases, especially when exposed to intermediate temperatures (600 – 900 °C) for extended periods. The formation of sigma phases significantly degrades both the material's toughness and its resistance to corrosion. As highlighted by (Knyazeva and Pohl, 2013), controlling rate after welding or heat treatment is essential to suppress these phases. Moreover, DSS requires careful control of phase balance. An excess of ferrite can reduce ductility and impact toughness, while excess austenite reduces SCC resistance. Proper solution annealing and quenching are necessary to restore the ideal duplex structure (Francis and Byrne, 2021).

## 1.8 Hydrogen Embrittlement in DSS

Hydrogen embrittlement (HE) is a serious degradation phenomenon in metals, happening especially in high-strength steels and stainless steels that are exposed to hydrogen-rich conditions. It happens when atomic hydrogen diffuses into the metal lattice, reducing its ductility and toughness, and ultimately resulting in an early brittle failure (Han *et al.*, 2023). This is a concern for duplex stainless steels (DSS) that are used in hydrogen transport, storage, and energy infrastructure.

### 1.8.1 Mechanism of Hydrogen Embrittlement in DSS

The susceptibility of DSS to hydrogen embrittlement is rooted in their duplex microstructure, which contains both ferrite (body-centered cubic, BCC) and austenite (face-centered cubic, FCC) phases. As said earlier, Ferrite allows faster diffusion of hydrogen, while austenite has higher solubility but slower diffusion rates. This combination creates complex hydrogen behaviour within the material, with ferrite acting as a fast path for transport and austenite acting as a trap (Knyazeva and Pohl, 2013).

Hydrogen embrittlement mechanisms in DSS include:

- a. **Hydrogen-enhanced localised plasticity (HELP):** According to (Lynch, 2011), hydrogen-assisted cracking (HAC) happened as a result of the solute hydrogen promoting dislocation movement. It was suggested that deformation was confined around fracture points as a result of solute hydrogen aiding dislocation activity, as hydrogen concentrations were localized near crack tips due to hydrostatic forces or hydrogen entrance at crack tips. It was then suggested that a more localised microvoid-coalescence (MVC) process than what would happen in inert conditions could thus cause sub-critical crack propagation. As seen in Figure 1.4, they postulated that fracture propagation happens via the coalescence of microcavities in the region of high hydrostatic stress and hydrogen concentration, which is far more localised than in an inert environment.

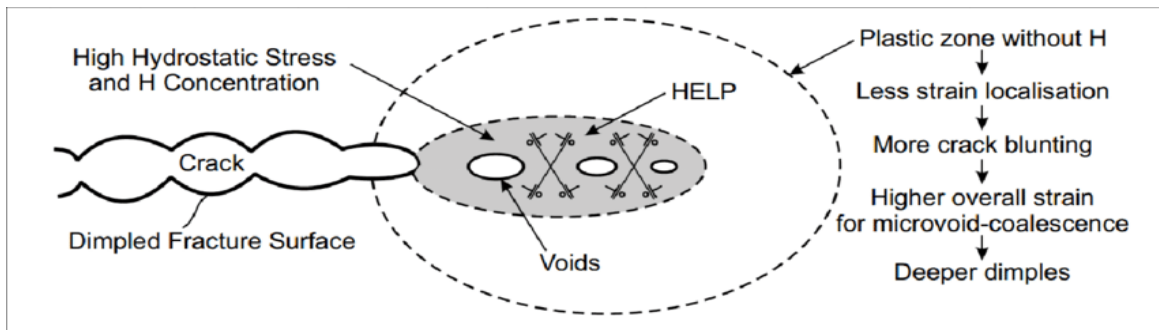


Figure 1.4: The diagrammatic representation of the HELP mechanism: the presence of hydrogen encourages dislocation mobility and localises plastic deformation at the crack tip; the microcavities in this area of high hydrogen concentration and hydrostatic stress coalesce to cause the crack to propagate (Tomoki, 2019).

**b. Hydrogen-Enhanced Decohesion (HEDE):** Typically, decohesion is thought of as a straightforward consecutive tensile separation of atoms upon reaching a critical crack-tip-opening displacement (CTOD), which is roughly half the interatomic distance (Lynch, 2011). HEDE describes that hydrogen reduces the binding strength between metal atoms. A high concentration of hydrogen at the grain boundaries or at other critical interfaces weaken the atomic bonds, thereby facilitating crack and propagating it. Decohesion may be accompanied by some dislocation activity, which might locally raise stresses at decohesion sites. However, this activity should be kept to a minimum to prevent the constant blunting of atomic sharp fracture ends. High concentration of hydrogen and the decohesion could happen at various locations, it could be at the atomically sharp crack tips which is due to the hydrogen's surface assimilation; it could also be at the several tens of nanometres ahead of cracks where dislocation shielding effects resulting to a maximum tensile-stress; the maximum hydrostatic stress position and the particle-matrix interfaces ahead of the cracks. (Lynch, 2011). According to (Lynch, 2011), there are no methods for directly monitoring atomic scale processes at fracture tips in bulk material, it is challenging to gain direct experimental proof of HEDE. The simpler field-evaporation of surface atoms seen during field-ion microscopy when hydrogen is employed as the imaging gas is arguably the most direct experimental proof that hydrogen may decrease interatomic interactions.

According to the Figure 1.5, showing the potential areas where the HEDE might appear; (a) near the crack tip where a high concentration of hydrogen is caused by plastic deformation and high hydrostatic stress; (b) a few tens of nanometres away from the crack tip where the dislocations' barrier effect results in a maximum hydrostatic stress; and (c) at grain-to-grain or precipitate interfaces up to several micrometres away from the crack tips.

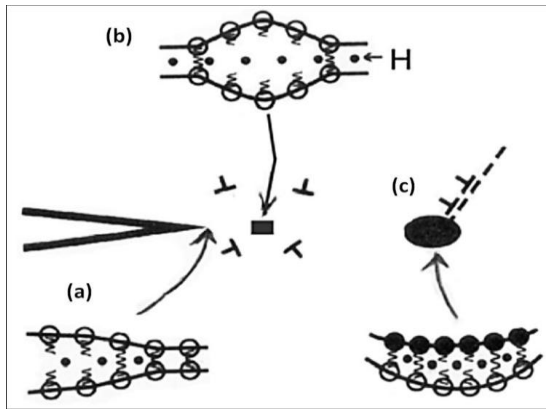


Figure 1.5: The diagrammatic representation of potential HEDE-producing zones (a) near the tip of the Crack; (b) a few tens of nanometres distant from the tip and (c) at grain to grain or precipitate to precipitate interfaces (Tomoki, 2019).

**c. Adsorption-induced dislocation Emission AIDE:** According to (Dwivedi and Vishwakarma, (2018)), which explains that this mechanism is essentially a hybrid of HEDE and HELP. This mechanism involves the surface adsorption of solute hydrogen atoms at the area of concentrated stress, such as fracture tips. Hydrogen adsorption at the crack tip causes the HEDE mechanism to degrade and the material's cohesive strength or interatomic link, while the HELP mechanism facilitates dislocation injection from the crack tip, which leads to fracture propagation via slip and microvoid formation. Decohesion and dislocation emission at the crack tip have caused the fracture to nucleate and expand in this way. This happens because of the combined effects of MVC and slide at the crack tip, cracks grew and fractured concurrently. High levels of adsorbed hydrogen on the surface of Fe, Ni, and Ti have been found to support the AIDE process. As shown in Figure 1.6.

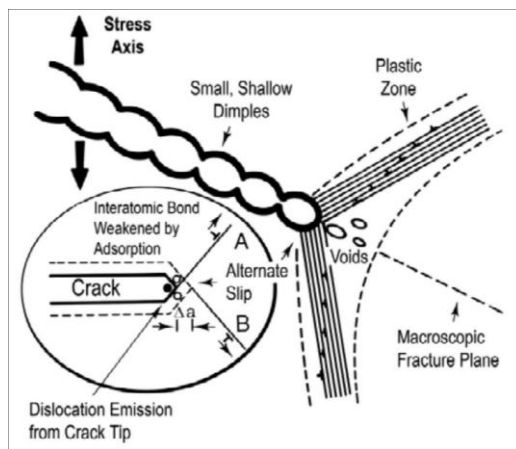


Figure 1.6: The AIDE mechanism is shown schematically. The two stages of embrittlement are the nucleation and growth of microcavities ahead of the crack tip and the local reduction of the material's cohesion energy, which encourages the nucleation and the emission of dislocations from the crack tip (Dwivedi and Vishwakarma, (2018)).

d. **Hydrogen-Enhanced Strain Induced-Void HESIV:** This was developed by using Thermal desorption Analysis TDA and hydrogen tensile tests with thermal aging. This concept is predicated on the idea that during plastic deformation, hydrogen in the material aids in the production and stabilisation of flaws. The overabundance of vacancies in the material, rather than the direct presence of hydrogen, is what causes the embrittlement of the metals. The crack growth process caused by void coalescence can be interpreted similarly to the HELP and AIDE processes, with the exception of the vacancy nucleation and growth phase (Tomoki, 2019).

While several mechanisms have been proposed to explain HE, this review will focus Primary on these four. This decision is based on the scope and space constraints of the current study.

### 1.8.2 Influence of Microstructure:

The ferrite-austenite ratio and grain boundary characteristics significantly influence hydrogen trapping and embrittlement behaviour. Knyazeva and Pohl (Knyazeva and Pohl, 2013), observed that DSS samples with a balanced and refined grain structure exhibited greater resistance to HE. On the other hand, coarse or irregular microstructures, or those containing sigma phase or secondary austenite, tend to be more susceptible to cracking due to hydrogen.

In addition, hydrogen prefers ferrite-rich zones for diffusion, but crack initiation frequently happens at the phase boundaries, where residual stresses and property mismatches are highest. This renders the welded joints, heat affected zones (HAZ) and cold-worked regions vulnerable.

According to Figure 1.7, in comparison to ferritic steel, austenitic materials are far more capable of solving hydrogen. In addition, compared to ferrite, the rate of hydrogen diffusion in austenitic iron is much lower.

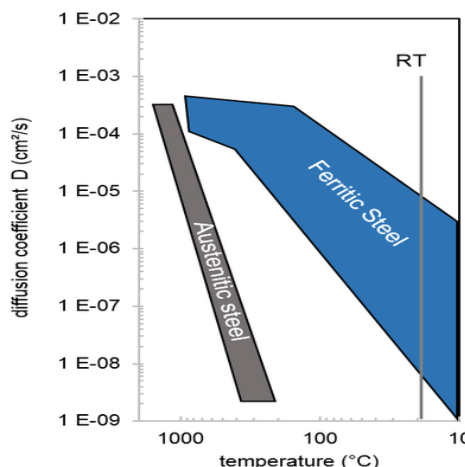


Figure 1.7: Hydrogen diffusion coefficient in ferrite and austenite depending on the temperature. (Klett and T. Hassel, 2020)

### **1.8.3 Testing and Assessment of Hydrogen Embrittlement in DSS:**

Hydrogen embrittlement is typically assessed using:

- Slow strain rate tensile testing (SSRT)
- Electrochemical hydrogen charging
- Fractography and Microscopy

Han et al. (Han *et al.*, 2023) highlighted that charging time, current density, and test environment significantly affect the degree of embrittlement observed. Post-charging mechanical testing reveals loss in elongation, increased hardness, and observation of fracture surfaces with brittle characteristics. Knyazeva and Pohl (Knyazeva and Pohl, 2013) used electron backscatter diffraction (EBSD) to map changes in grain orientation and cracking, correlating texture evolution with embrittlement susceptibility.

Now the hydrogen embrittlement test methods are described thus:

#### **a. Slow Strain Rate Testing (SSRT)**

During this test, an ever-increasing elongation is applied over time until the specimen fails or fractures at very low strain rates. (Dwivedi and Vishwakarma, (2018)).

The SSRT's ISO 7539 Part 7 a Corrosion of metals and alloys-stress corrosion testing; ASTM G129 a standard practice for slow strain rate testing to evaluate the susceptibility of metallic materials to environmentally assisted cracking and NACE TM0198 standards a slow strain rate test method for screening corrosion resistant alloys for stress corrosion cracking in sour oilfield service, have been in use for ten to twenty years, albeit they have undergone adjustments throughout that period. They all offer useful details about the test and associated topics like safety. The following are some ways that these standards differ (Henthorne, 2016):

- a. NACE TMO198 is designed for CRAs (stainless steels and high nickel alloys) in sour oilfield service, but it offers information that is helpful for other SSRTs.
- b. For a fully effective utilisation, all three require citation to other standards; nevertheless, ISO 7539 Part 7 is the least stand-alone and NACE TM0198 the most.
- c. The most useful advice on specimen preparation, tensile test equipment, data reporting, and others, may be found in NACE TM0198, for example, it warns against applying compressive pressures from thermal expansion during the pre-tension phase.
- d. Both bending and axial tensile stress are permitted by ISO 7539 Part 7, but the axial tensile stress is often assumed.

e. NACE TM0198 and ISO 7539 Part 7 do not permit fatigue pre-cracked specimens, ASTM G129 does, albeit Part 9 does.

f. While ISO 7539 part 7 permits a quicker strain rate during the elastic range and a decrease in the plastic range, ASTM G129 permits an interrupted SSRT at extremely slow rate ( $10^{-8}\text{s}^{-1}$ ), which may result in an increase in the strain rate (Henthorne, 2016).

SSRT assesses DSS that is sensitive to hydrogen embrittlement by mechanical loading in uniaxial stress of specimens at a strain rate of  $10^{-6}$  to  $10^{-7}\text{s}^{-1}$  in both air and hydrogen environments. Fracture behavior, reduced ductility, and brittle modes signal embrittlement (Francis and Byrne, 2021). Engineering stress-strain curves for Fe, Fe-0.02C, and Fe-0.1C materials with and without in-situ hydrogen charging are displayed in Figure 1.8.

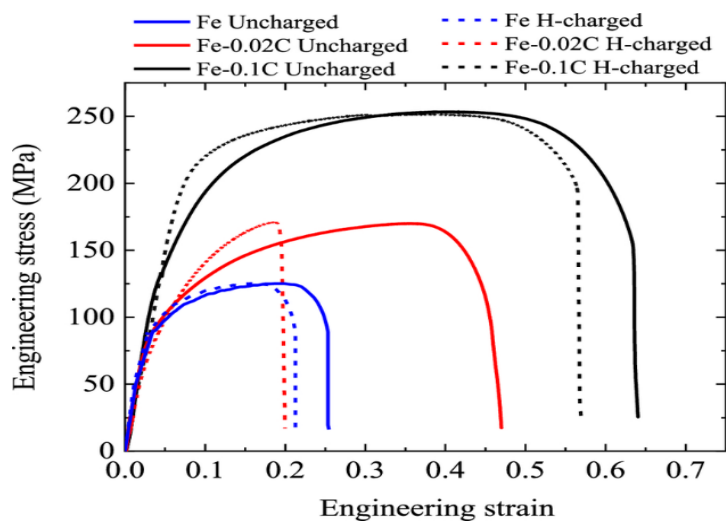


Figure 1.8: Changes in engineering stress-strain curve with and without in-situ electrochemical hydrogen charging at the strain rate of  $3.4 \times 10^{-6}\text{s}^{-1}$ . Source: (Pichler *et al.*, 2023)

The amount of cementite in the alloy increases as the carbon concentration grows. The alloy's yield strength and ultimate tensile strength rise when increasing carbon content because the cementite is tougher than the ferrite matrix. Because of testing in air, this increase in strength is followed with a rise in elongation at fracture and, thus, increased toughness. The higher rate of work hardening during the Fe-0.02C specimen, followed by the Fe-0.1C specimen, indicates that the sample has become more resilient because of the higher percentage of pearlite particles and carbon content. Furthermore, when the test environment was altered, each specimen's yield strength and ultimate tensile strength essentially stayed the same (Pichler *et al.*, 2023).

### b. Hydrogen Permeation test:

The most straightforward method of measuring hydrogen diffusion constant in steel is permeation testing. The permeation test in steel has been successfully implemented by combining it with other methods. This permeation test is essentially a double-cell setup, with an oxidation cell (exit cell) in one chamber and an entering cell (also known as a charging cell) in the other. A thin steel sheet specimen divides these two cells. Hydrogen charging has been accomplished by the electrochemical technique.

According to the Figure 1.9, a 1mm thick sample was positioned between the hydrogen charging and hydrogen releasing cells during hydrogen permeation, and the sample and solution had a  $7.065\text{cm}^2$  (30mm in diameter) contact area on both sides.

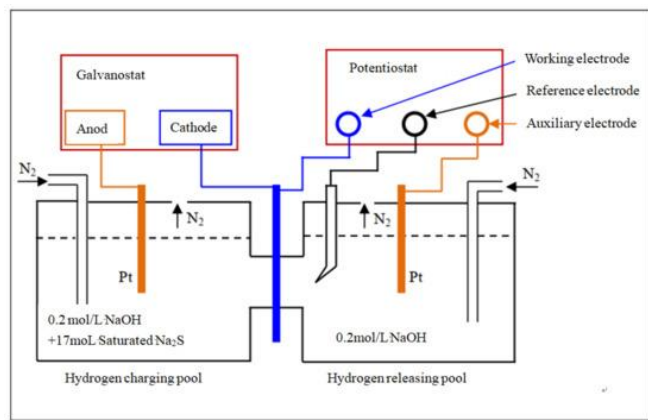


Figure 1.9: Schematic diagram of hydrogen permeation test device. (Li *et al.*, 2023).

The anode side of the sample, which releases hydrogen, was nickel-free. To eliminate oxygen, nitrogen was continually added to both electrolytic cells. To keep the steel substrate from oxidising, the anode side was coated with nickel. The potentiostat's settings were adjusted to place the sample at potentiostatic polarisation with a steady potential of 250 mV.

In order to encourage hydrogen penetration into the steel, the hydrogen charging current at the hydrogen charging side was tuned to  $4\text{ mA/cm}^2$  once the residual current at the anode side had stabilised. The initial hydrogen charging procedure was finished after the anode side current reached a steady level. The anode side current then began to drop once the hydrogen charging current was reduced to zero. The second hydrogen charging began after the anode side current returned to a steady level. The initial experiment's hydrogen charging settings were identical to this one. Following that, it was possible to retrieve the anode side current curve as it changed over time (Li *et al.*, 2023).

### c. Thermal Desorption Analysis (TDA)

TDA determines the hydrogen content by heating the sample and by monitoring the desorbed hydrogen gas. It provides information about embrittlement concerns by differentiating between diffusible and trapped hydrogen (Francis and Byrne, 2021).

One of the most widely accepted methods for studying HE and Hydrogen-induced failure is Thermal desorption spectroscopy TDS, also known as Thermal Desorption Analysis. The amount of diffusible hydrogen in steel and the role of hydrogen in failure may be determined using a variety of methods, according to the literature. Another significant factor in HE is hydrogen mobility. The diffusible hydrogen can be qualified and quantified using TDA (Dwivedi and Vishwakarma, (2018)).

The TDA technique uses controlled and regulated heating to measure the amount of desorbed hydrogen. Steel has traps, and it is these traps that causes hydrogen buildup.

When steel is heated, hydrogen absorbs the thermal energy and releases it when the energy absorbed reaches a threshold level equivalent to the desorption activation energy. Thus, the temperature at which hydrogen atoms are released is known as the desorption temperature. Quadrupole mass spectroscopy is used to measure the amount of desorbed hydrogen (Dwivedi and Vishwakarma, (2018)).

The Figure 1.10 shows the TDA schematic diagram, its exceptional sensitivity and ability to quantify the little amount of desorbed hydrogen more precisely than other methods make it special.

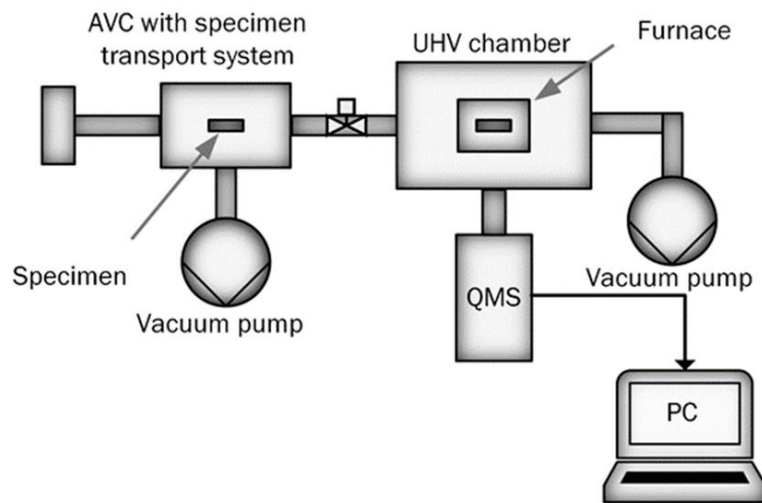


Figure 1.10: Schematic diagram of Thermal Desorption Analysis (Fangnon et al., 2020).

High HE detention and a deeper comprehension of the HE process can be obtained by combining the TDA approach with additional tests (Dwivedi and Vishwakarma, (2018)). Figure 1.11 shows the TDA curves corresponding to measurement procedures.

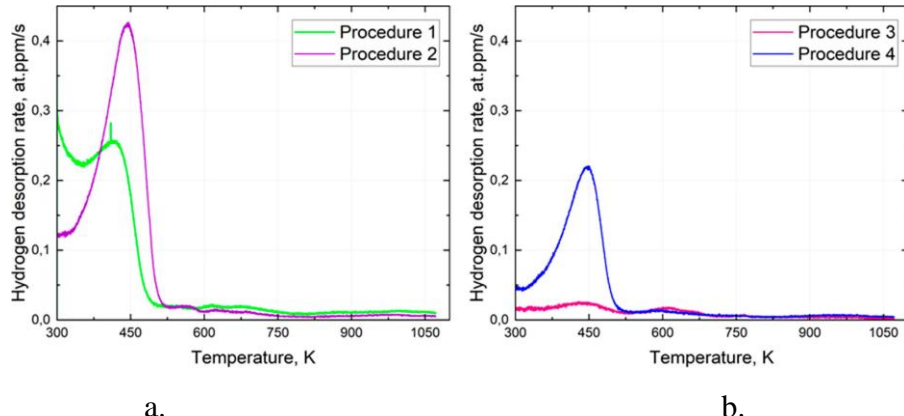


Figure 1.11: TDA curves corresponding to measurement procedures 1,2, with the same AVC dwelling time which is 15 minutes (a) and Procedure 3, 4, with the same AVC dwelling time which is 60 mins on (b) (Fangnon *et al.*, 2020).

The hydrogen TDA analysis was used to examine the hydrogen redistribution in the steel. During the approximate 15 minutes absolute vacuum conditions (AVC) residence period, there was a notable hydrogen redistribution within the sample material, as seen by the rediffusion signal (RDS) data obtained using measuring techniques 1 and 2. The AVC refers to the vacuum system where the sample is kept under absolute value conditions before heating begins. This is to allow hydrogen inside the steel to distribute before the actual desorption measurement starts. The RDS captures the redistribution of hydrogen within the material from that AVC residence time.

As demonstrated, pre-cooled specimens have an initial hydrogen desorption rate that is nearly three times lower than that of uncooled specimens when tested at room temperature. For measurement techniques 3 and 4, the dynamic of the hydrogen thermal desorption rate change is likewise varied, presumably due to a variable distribution of hydrogen across the steel's trapping sites. It is evident that cooling the specimen holder to 213 K not enough to completely stop the diffusion of hydrogen in the steel under study (Fangnon *et al.*, 2020).

#### d. In-situ SSRT with Electrochemical Charging

Combining SSRT with live hydrogen charging gives a realistic assessment of hydrogen-assisted cracking during service. This technique is particularly effective for assessing hydrogen-induced fracture behaviour in DSS (Francis and Byrne, 2021).

According to Figure 1.12: In-situ SSRT schematic showing loading and Hydrogen charging system. Source: (Fu et al., 2020), the specimen served as the cathode and the platinum sheet as the anode during in-situ hydrogen charging.

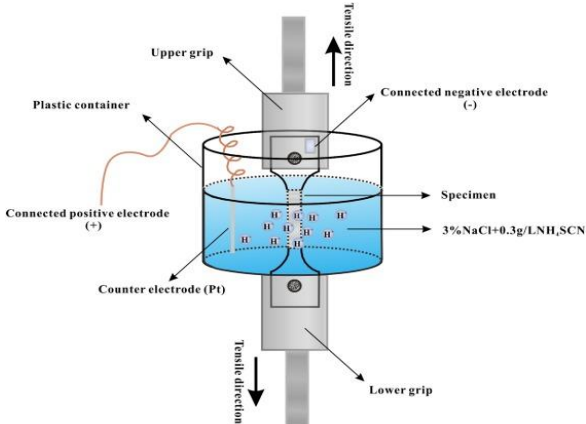


Figure 1.12: In-situ SSRT schematic showing loading and Hydrogen charging system. Source: (Fu et al., 2020)

In contrast to hydrogen pre-charging, which is more representative of the actual service scenario, hydrogen could be efficiently delivered into the sample without generating surface defects since the hydrogen bubbles were equally deposited on the sample surface.

In order to study the surface morphology using a scanning electron microscope SEM following the in-situ hydrogen charging experiments, the sample surface was meticulously polished prior to the testing. To get accurate findings, three samples were examined in each circumstance (Chen et al., 2023).

#### 1.8.4 Mitigation Approaches:

Several techniques are employed to lessen hydrogen embrittlement in DSS:

- Microstructure optimization: By preserving balanced phase ratios and removing intermetallic phases like sigma.
- Surface engineering: By using coatings to lessen the infiltration of hydrogen.
- Environmental control: By minimizing cathodic overprotection or chemical exposure that promotes hydrogen absorption.
- Post-weld heat treatment (PWHT): To ease residual stresses and lower hydrogen concentration.

When designing DSS for hydrogen service, a careful material selection, process control, and environmental awareness are considered to reduce the possibility of embrittlement.

In this chapter, the history, structure and properties of DSS was explored, with a focus on their response to hydrogen environments. Reviewing the mechanisms of hydrogen embrittlement, testing methods and mitigation strategies. The main attention is that DSS offers strength and corrosion resistance, its dual phasic nature also makes it vulnerable to hydrogen, and understanding this is critical to its safe application.

# **CHAPTER II:**

# **MATERIAL AND METHOD**

## 2.0 MATERIAL AND METHODS

### Introduction

In this chapter, the materials, equipment, and the experimental procedures employed in this research will be outlined to investigate the hydrogen embrittlement in duplex stainless steels. The experiments in this research were conducted at the steel institute (IEHK) at the RWTH University, Aachen, where the advanced material testing and hydrogen analysis equipment are available. All mechanical testing were carried out using the facilities of this Laboratory, while the thermal desorption and the elemental analysis were conducted using instrumentation provided at the Research Centre for Digital Photonic Production RCDPP which shared an extension with IEHK Laboratory. The study focused on duplex stainless steels which is commonly used in energy and chemical processing industries due to their corrosion resistance and mechanical strength.

### 2.1 Materials and Chemical Composition

The material under investigation was the duplex stainless steel S82441, which has a balanced dual-phase microstructure made up of austenite and ferrite. Samples for the research were prepared according to the standard metallurgical procedures which involve machining to dimension as seen in Figure 2.1, sectioning, grinding, polishing and cleaning to get rid of any surface impurities. The chemical composition of the material was taken from delivered data sheet of the supplier Swiss Steel Group, ensuring the accurate measurement of oxygen, hydrogen and other alloying elements. As seen in Figures 2.2 and 2.3, the preparation made sure that the specimens met ASTM E8/E8M requirements (BSSA, 2025) for tensile testing emphasizing the areas intended for hydrogen charging and protection.

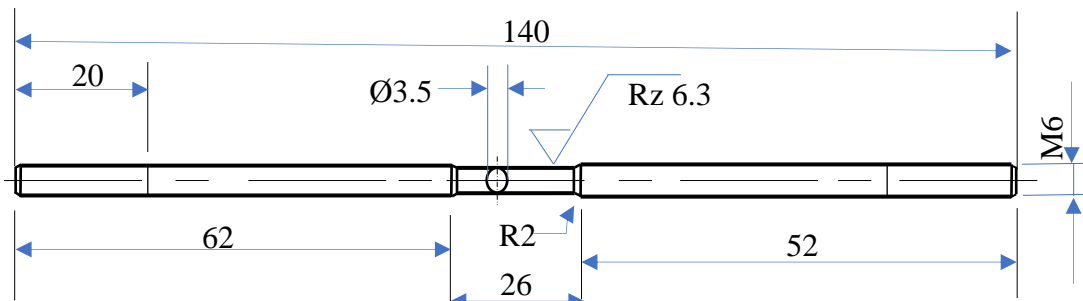


Figure 0.1: Dimension of the tensile test sample

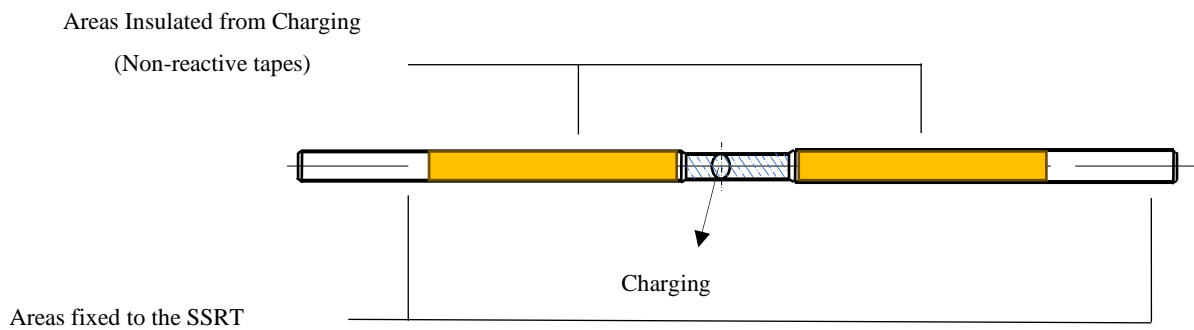


Figure 0.2: The tensile test sample, indicating the charging area



Figure 0.3: The test sample

## 2.2 Metallographic Preparation

To ensure a clean and smooth surface, all specimens were metallographically prepared before mechanical testing and hydrogen charging. To obtain a polished finish, this procedure first entailed grinding then polishing and etching (Gunn, 1997). In order to eliminate any remaining abrasive particles or rough surfaces, also to avoid contamination that would impede the hydrogen absorption process. The polished specimens were cleaned in ethanol. This preparation made it possible to reliably correlate mechanical performance with microstructure characteristics and guaranteed accurate test results. The images below show the metallographic procedures.



*Figure 0.4: The specimen before the grinding process*



*Figure 0.5: The Saphir M1 Grinding and Polishing machine*

Using the Saphir M1 device, the grinding of the specimen begins, with a tap water used as a grinding medium, having set the speed to 300 rpm, the sample are ground on a P80 SiC (Silicon Carbide) paper which is the coarsest and gradually graduates to further grinding steps with P240, P320, P500, P800, P1200 and P2400 which is the finest paper we used to get the best result. The samples are always rotated at 90° between the individual sanding steps. After surface grinding, the samples are rinsed under running water and then cleaned in an ultrasonic bath in a beaker that is filled with ethanol for 1-2mins and dried under the dryer.



Figure 0.6: The SiC papers

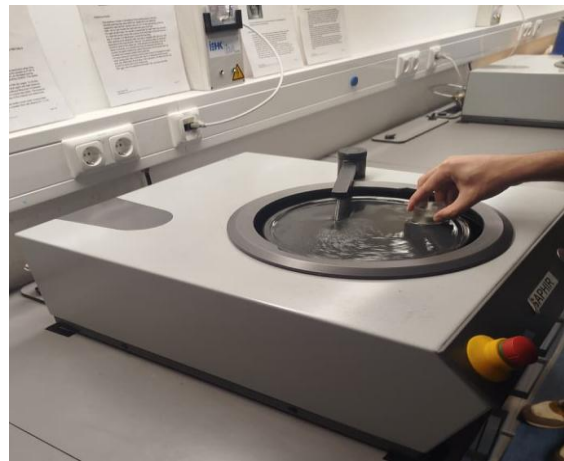


Figure 0.7: During grinding procedure



Figure 0.8: An ultrasonic cleansing beaker



Figure 0.9: The dryer

The Polishing Process: Using the Saphir M1 device, the polishing process entails that the maximum number of revolutions of the sanding disc is 150 rpm. For duplex steels, we have a specific grade that is used in polishing it. Some diamond suspensions at 3  $\mu\text{m}$  and 1  $\mu\text{m}$  with a coolant is used by spreading a few mL of it on the appropriate polishing for like 3 minutes. After the 1  $\mu\text{m}$  polishing step, no scratches are expected to be seen with the naked eyes. Then cleaned again ultrasonically using ethanol.



Figure 0.10: Diamond suspensions



Figure 0.11: Polishing procedures



Figure 0.12: Specimen after polishing

The etching procedure: The specimen was first polished, cleaned and then placed inside a solution of 1000ml of warm distilled water, 200 g of ammonium bifluoride and 5g of Potassium disulfide, for 3 minutes to allow visibility of boundaries and distribution of ferrite and austenite under Optical microscope or scanning electron microscope (SEM).



Figure 0.13: Etching procedure inside the solution

## 2.3 Electrochemical Hydrogen Charging

The manufactured tensile specimens were submerged in an acidic electrolyte solution containing 0.05M Sulphuric acid ( $H_2SO_4$ ) in order to perform electrochemical hydrogen charging. Each specimen serves as a working electrode during charging. In order to encourage the diffusion process of hydrogen into the material, a steady current density was provided. As shown in Figures 2.2 and 2.14, a non-reactive insulating tape were used to safeguard regions not meant for charging. For proper hydrogen intake optimisation and to simulate the circumstances that may cause embrittlement, the hydrogen charging was carried out right before the tensile test.



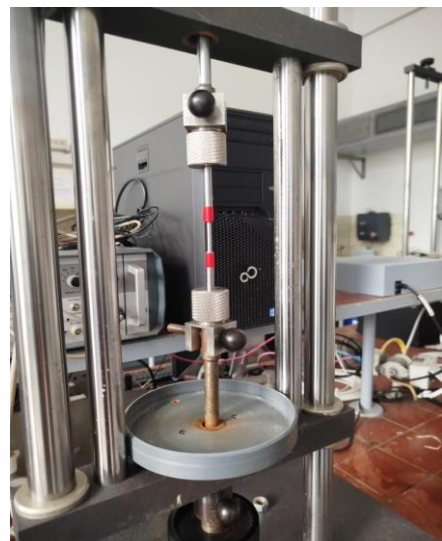
Figure 0.14: The test sample with the non-reactive insulating tapes

## 2.4 The Slow Strain Rate Test

As shown in Figure 0.15 a and b, the material testing system was used to perform the slow strain Rate Test (SSRT). The tests were conducted in two distinct environments: the in-situ hydrogen charging and the ambient air at a regulated temperature of around 21°C. With a constant speed of 11mm per day,  $1.273 \times 10^{-4} mms^{-1}$  (per second), each specimen was subjected to a strain rate of  $5 \times 10^{-6} s^{-1}$  in order to assess its tensile characteristics and vulnerability to hydrogen embrittlement. Stress-strain curves, yield strength, ultimate tensile strength, elongation at break, and time to failure were among the data that recorded during the test. So as to be able to simulate real word exposure scenarios where mechanical loads and hydrogen infiltration happens simultaneously. The in-situ SSRT used simultaneous tensile loading and electrochemical hydrogen charging as seen in Figure 0.17 and Figure 0.18.



a.



b.

Figure 0.15: Material testing equipment (a) Before set-up (b) During SSRT setup



Figure 0.16: Non-reactive tape

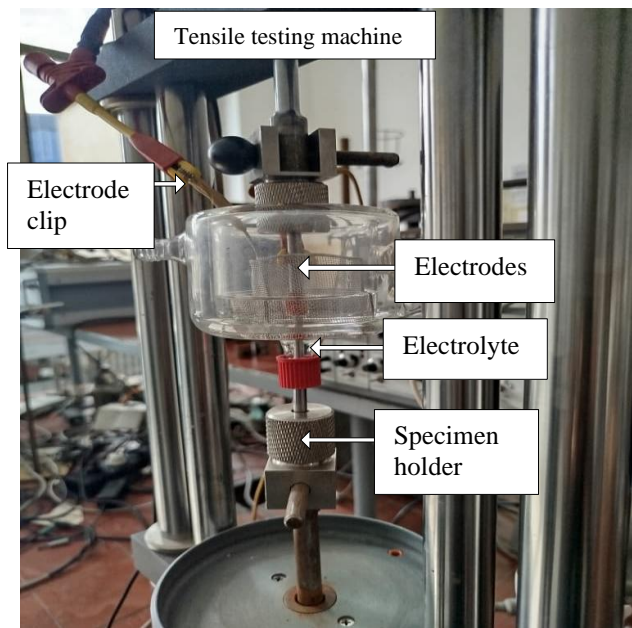


Figure 0.17: The In-situ SSRT Setup



Figure 0.18: Complete *in-situ* SSRT setup

According to Figure 0.17, the positive electrode is attached to the platinum while the negative terminal is attached to the sample. From the sulphuric acid solution, the hydrogen ion  $H^+$  goes to the sample which is negatively charged so that hydrogen can concentrate on the sample, this is done for practical purposes. At the top of the machine, is the force sensor as shown in Figure 0.18, which measures the Force being applied.

## 2.5 Hydrogen Analysis (TDA)

Following the SSRT, Thermal desorption analysis (TDA) was carried out in order to measure the amount of hydrogen that was retained in the specimens and also to describe the types of hydrogen trapping sites. The Bruker IR07 analyser, shown in Figure 0.19, was used to perform the measurements. In a Nitrogen carrier gas atmosphere, each specimen was heated under control to  $800^{\circ}C$  at  $0.3$  K/s heating rate. Desorption profiles showing the peak release temperatures are diffusible hydrogen concentration were produced by continually detecting and recording the released hydrogen during heating.

The Mettler Toledo ME204 analytical balance is used to measure the weight of the specimen.

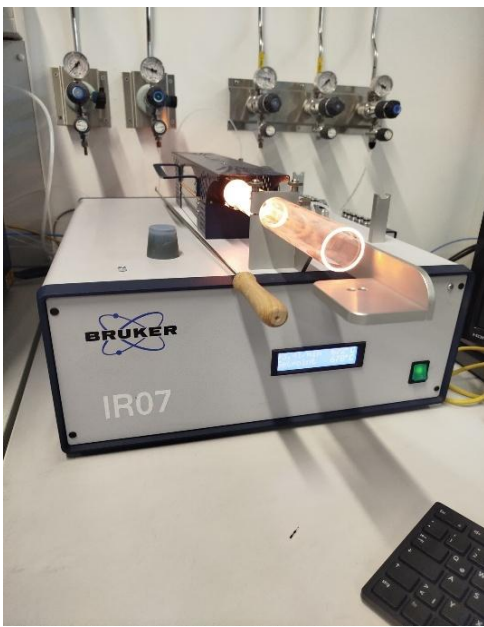


Figure 0.19: BRUKER IR07 Analyzer

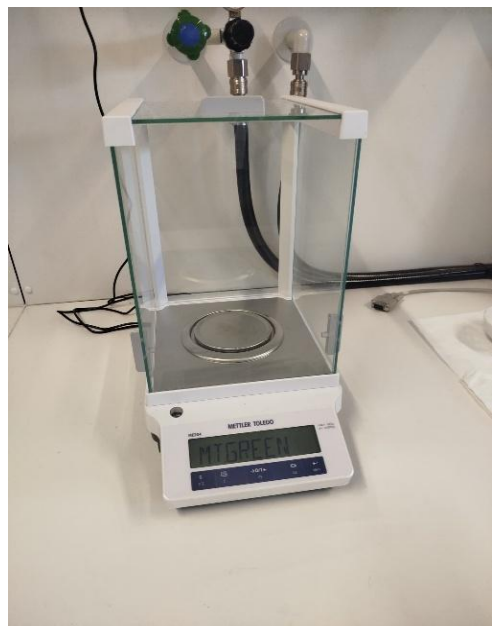


Figure 0.20: Mettler Toledo ME204 analytical balance

## 2.6 Data Processing and Analysis

The proprietary software of the testing system for the mechanical performance analysis and the Bruker IR07 software for the thermal desorption curve creation were used to process the experimental data gotten from SSRT and TDA. To assist in the interpretation of the findings, statistical analysis and graphing were carried out using MATLAB and Microsoft Excel. In addition, fractured surfaces and microstructural alterations caused by hydrogen exposure were investigated using microscope analysis, including optical and scanning electron microscopy. To be able to determine the impact of hydrogen on the mechanical integrity of duplex stainless steels, all the results were correlated.

This chapter provides materials, tools and methods employed for the investigation of hydrogen embrittlement of duplex stainless steels. A comprehensive approach which includes the sample preparation to the Slow Strain Rate Test, the In-situ SSRT, and the Thermal Desorption Analysis was used to assess mechanical degradation and hydrogen interactions. Data collection and analysis frameworks were mentioned, and the data representations will be examined and discussed in the next chapter.

# **CHAPTER III:**

# **RESULTS AND DISCUSSION**

## 3.0 RESULTS AND DISCUSSION

### Introduction

This chapter shows the findings gathered from the experimental procedures that was discussed earlier in Chapter 2. The results are structured to reflect the techniques used; The experiments reveal the chemical analysis, metallographic observation, fractographic evaluation, SSRT, In-situ SSRT under hydrogen Charging, TDA. These findings were discussed in terms of their significance to the understanding of hydrogen embrittlement in DSS.

### 3.1 Chemical Composition

Using an industrial material, with the chemical composition standards as indicated below:

*Table 0.1: Chemical composition of duplex Stainless steel*

UNS	EN	Cr	Ni	Mo	N
S82441	1.4662	24	3.6	1.6	0.27

The composition above confirms the material's classified as a duplex stainless steel, with a balanced amount of ferrite and austenite stabilizing elements to ensure resistance to corrosion and strength.

### 3.2 Microstructural Analysis (Metallography)

Using an Optical microscope, the microstructure of the material in as received condition is presented in Figures 3.1 and 3.2 after grounding, polishing and etching.

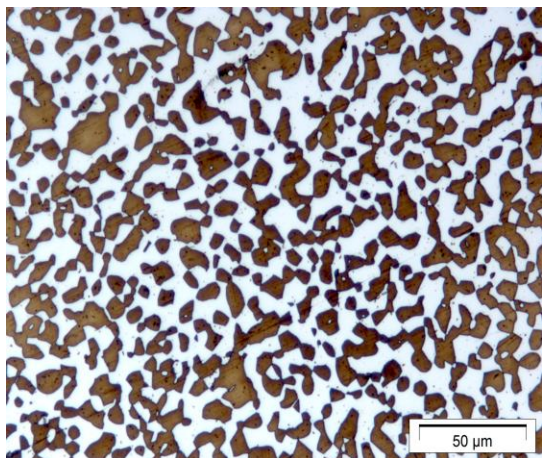


*Figure 0.1: Microstructural analysis at 500X magnification*

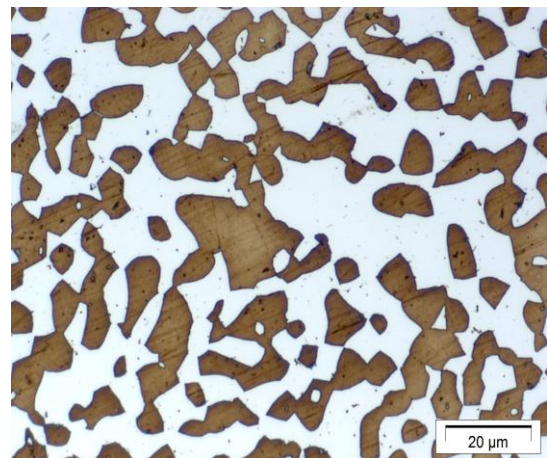
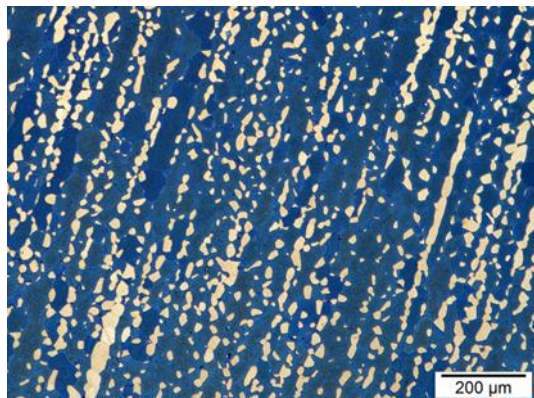


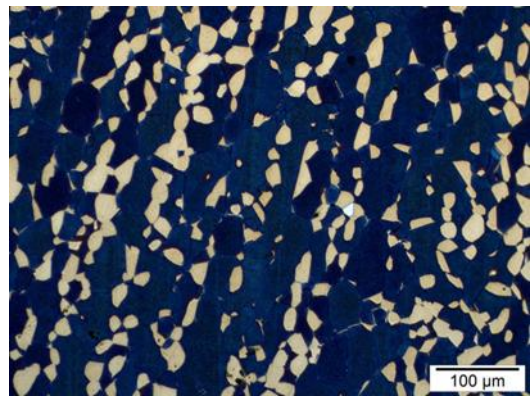
*Figure 0.2: Microstructural analysis at 1000X magnification*

To change the austenite-ferrite volume fractions a heat treatment at 1250 °C for 90 minutes in a muffle furnace is applied. The microstructure is shown in Figures 3.3, showing ferrite (light phase) and austenite (dark phase). Austenite appeared as small patches scattered throughout the ferrite background.



a

Figure 0.3: Microstructure at 1250 °C, 90 mins 100X magnification



b

Figure 3.3: Microstructure at 1250 °C, 90 mins 200X magnification

The microstructure clearly show that the two phases (ferrite and austenite) are evenly and finely spread throughout the material. The heat treatment helped some of the ferrite turn into austenite, leading to a better phase balance. This kind of microstructure is important because it affects how the material reacts when exposed to hydrogen, including how easily hydrogen gets trapped and where it might cause damage.

### 3.3 Mechanical Testing

#### 3.3.1 SSRT in Air (without hydrogen charging)

The SSRT was conducted under the ambient conditions to establish the baseline mechanical properties of the DSS. The stress-stain curve shows a typical ductile behaviour, necking and significant elongation before it fractures. Here we have the following values:

The yield Strength: 577 MPa

Ultimate Tensile Strength: 740 MPa

Elongation: 38 %

Time of Fracture: 64113.5 s

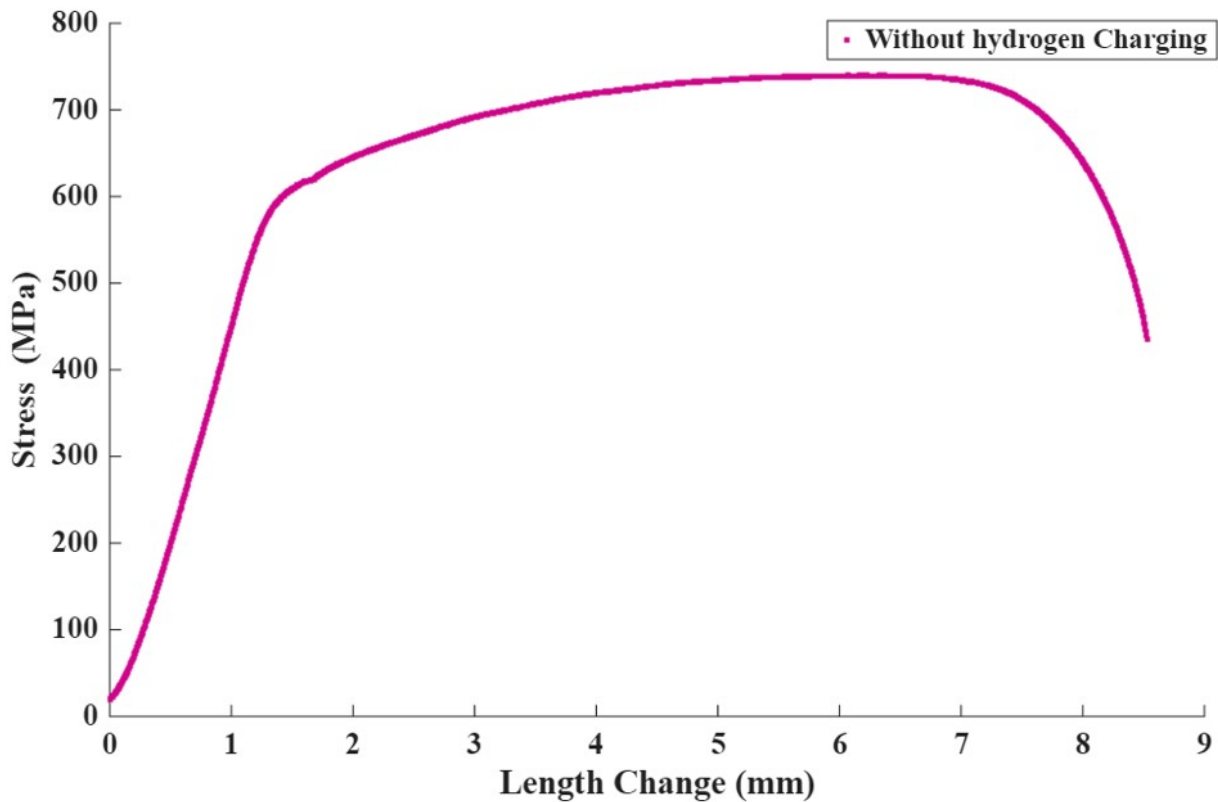


Figure 0.4: Stress-length change curve of DSS in-Air

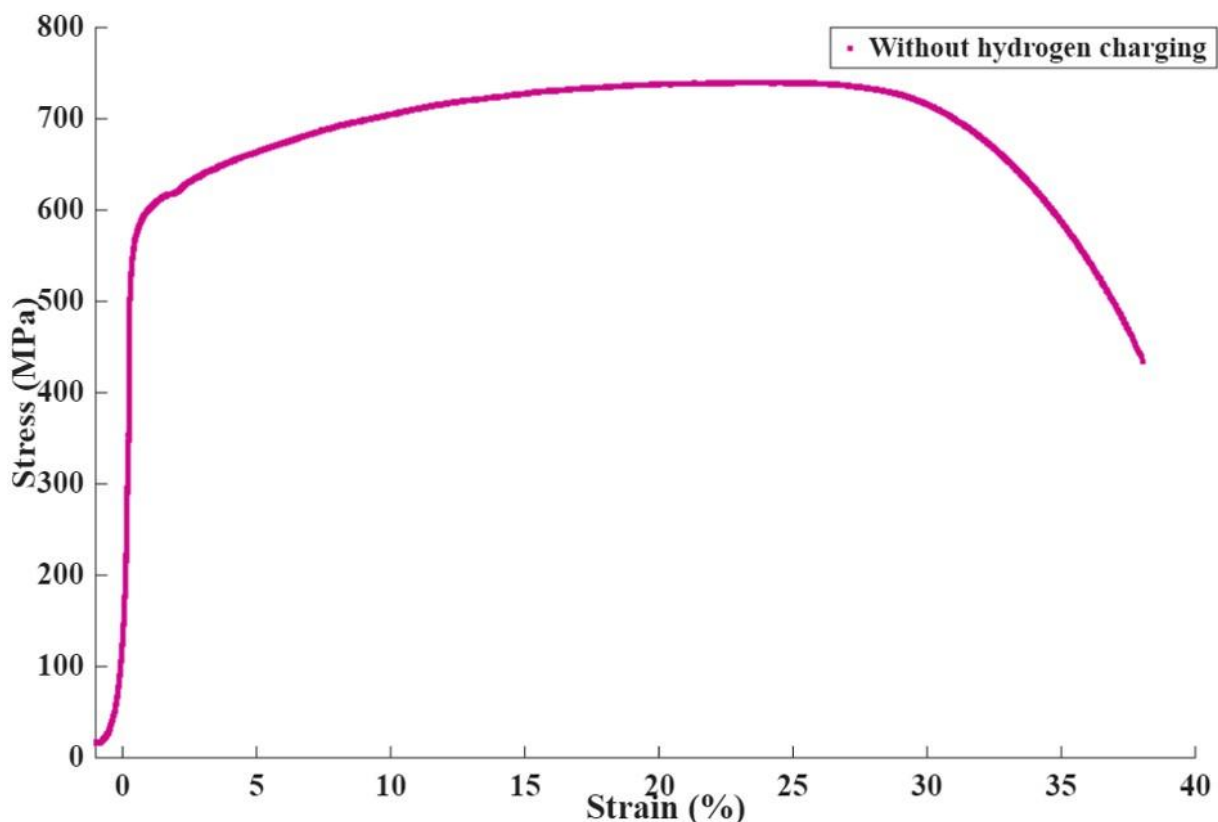


Figure 0.5: Stress-strain curve of DSS in-Air

The above curve indicates a tensile behaviour of the duplex stainless steel tested in-air, that is,

without hydrogen exposure. The curve follows the typical ductile metal reaction, linear elastic region, continuous yielding, strain hardening, and necking before fracture.

It was observed that both the yield strength and ultimate tensile strength were found to be high, which is in line with DSS's dual phase microstructure. The elongation of fracture is also significant, which confirms the high ductility in the absence of hydrogen. As a result, this material performs exceptionally well in mechanical performance in inert conditions. It showed good toughness, strength and ductility.

### 3.3.2 In-Situ SSRT under Hydrogen Charging

The in-situ SSRT system combined tensile testing with electrochemical hydrogen charging using a 0.05M sulphuric acid ( $H_2SO_4$ ) solution. A platinum electrode and the sample served as the working electrode was adopted to maintain current density, thereby promoting hydrogen absorption. Figures 3.6 and 3.7 are showing the SSRT results with hydrogen charging. Hydrogen charging significantly reduced elongation and time to failure with brittle fracture behaviour observed.

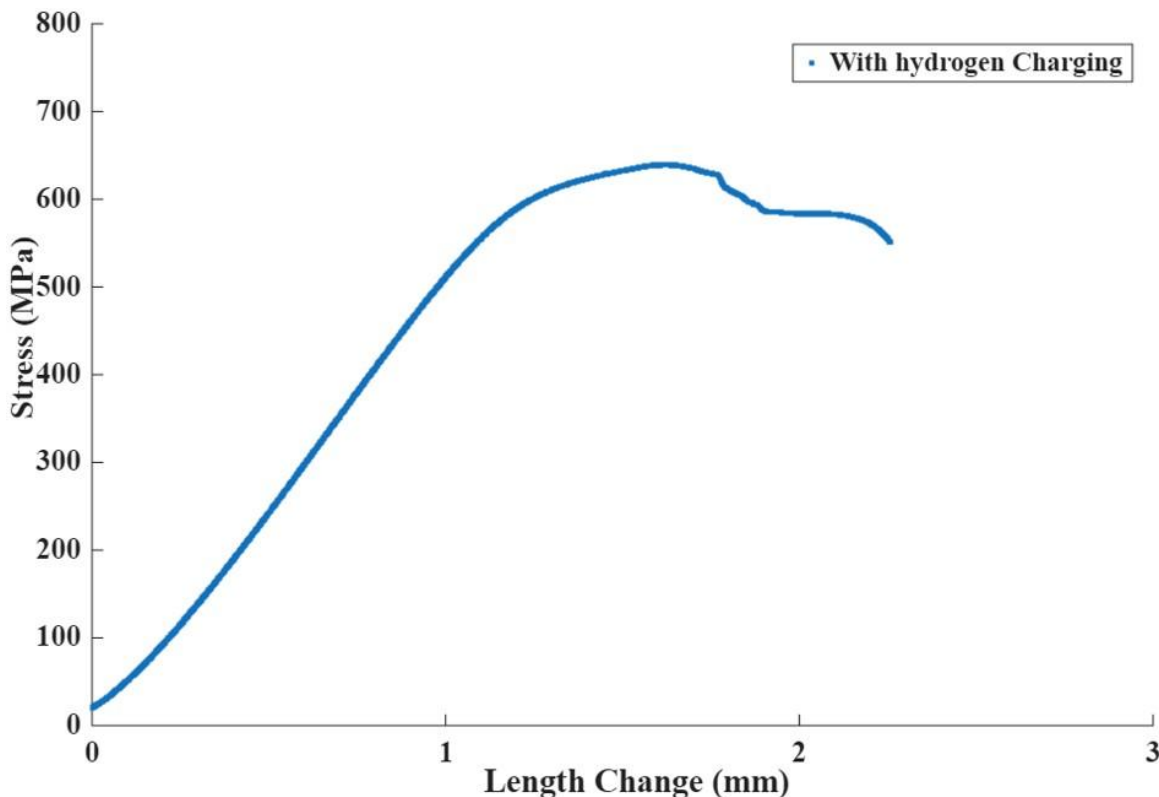


Figure 0.6: Stress-length change curve under hydrogen charging

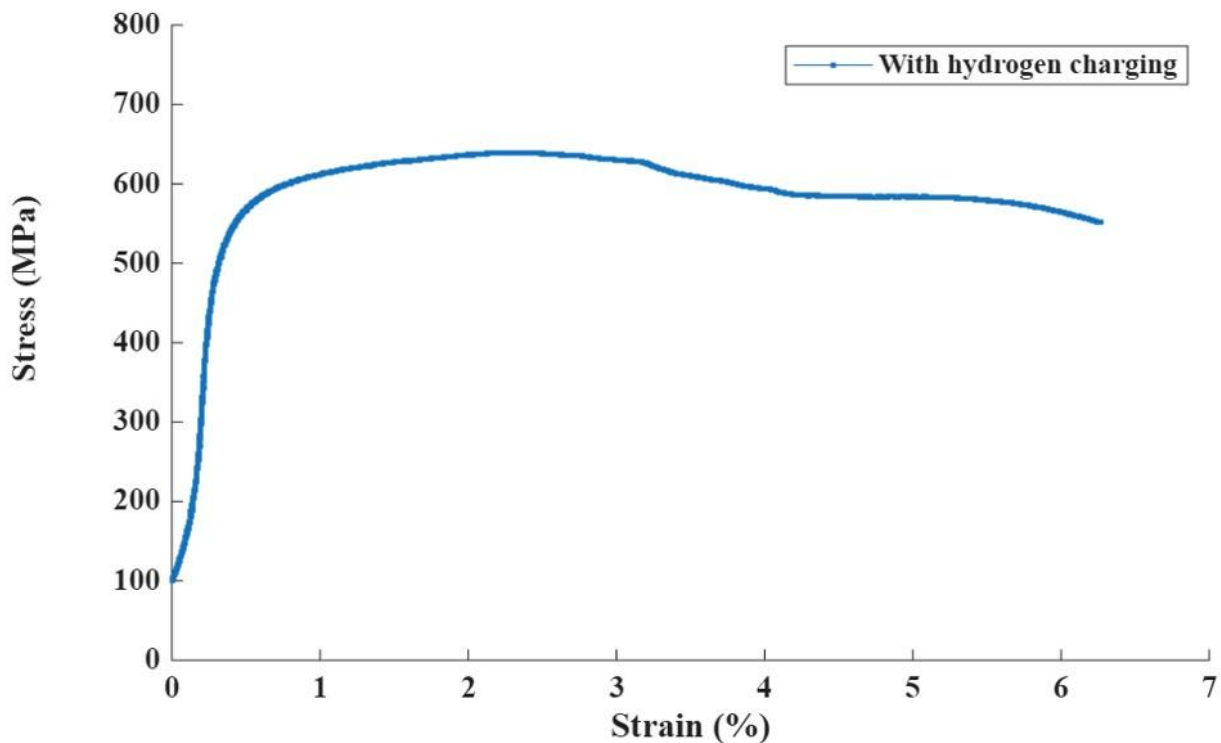


Figure 0.7: Stress-Strain Curve under Hydrogen Charging

### 3.4 Thermal Desorption Analysis (TDA)

TDA was conducted to measure the hydrogen content and trapping behaviour in the charged samples. The analysis was performed by heating up to 800°C at a rate of 0.3 K/s with nitrogen as a carrier gas. Nitrogen was used because it acts as an inert carrier gas under this test conditions, which means it does not react with the sample or the hydrogen that was released during heating, so as to prevent unwanted chemical reactions like oxidation by displacing oxygen from the system. This is why it is preferred to argon in this test condition.

Peaks observed in the TDA curve indicate desorption of diffusible and trapped hydrogen.

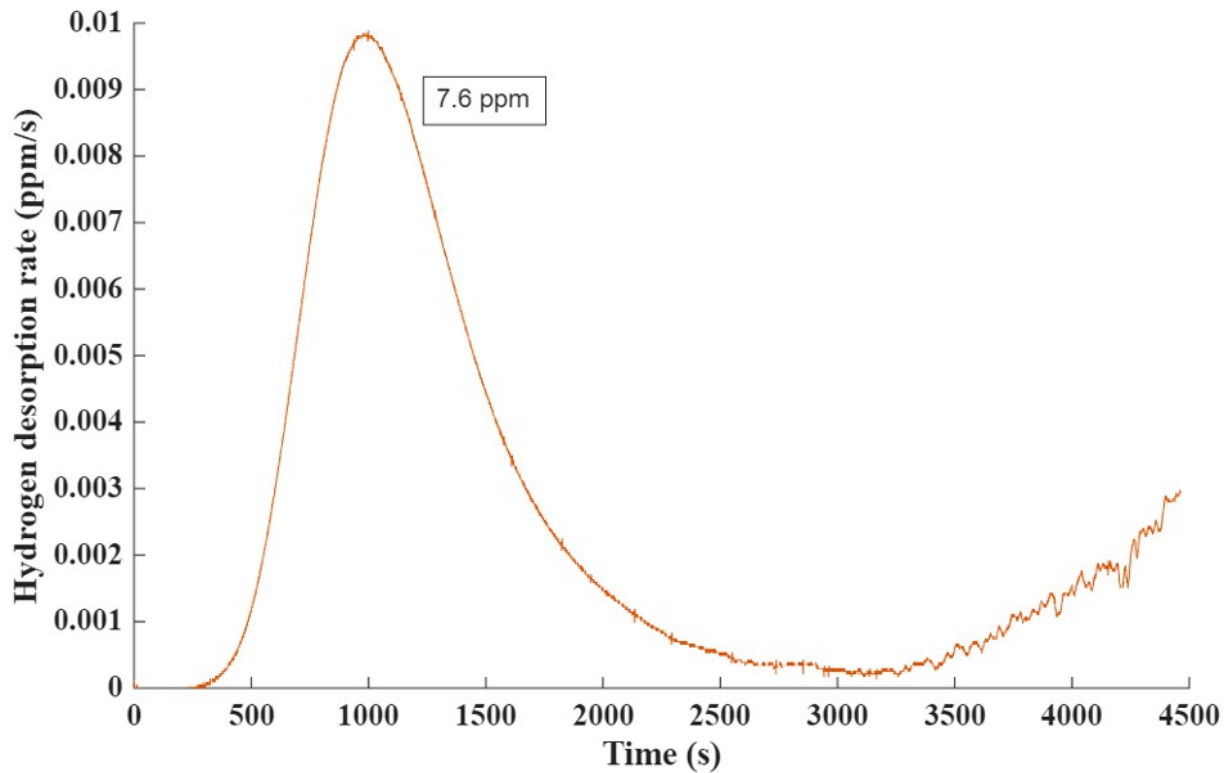


Figure 0.8: TDA desorption over Time

Figure 3.8 illustrates the gradual emission of hydrogen during heating. At the beginning, there are weak traps, the later time indicated strong traps. This demonstrates that by determining the temperature, the steel can be heated to that point before being used, a process known as bake-out or hydrogen degassing. The steel will be less likely to fail when utilized in hydrogen rich environments because the heat pushes out the hydrogen that may develop cracks later in the material.

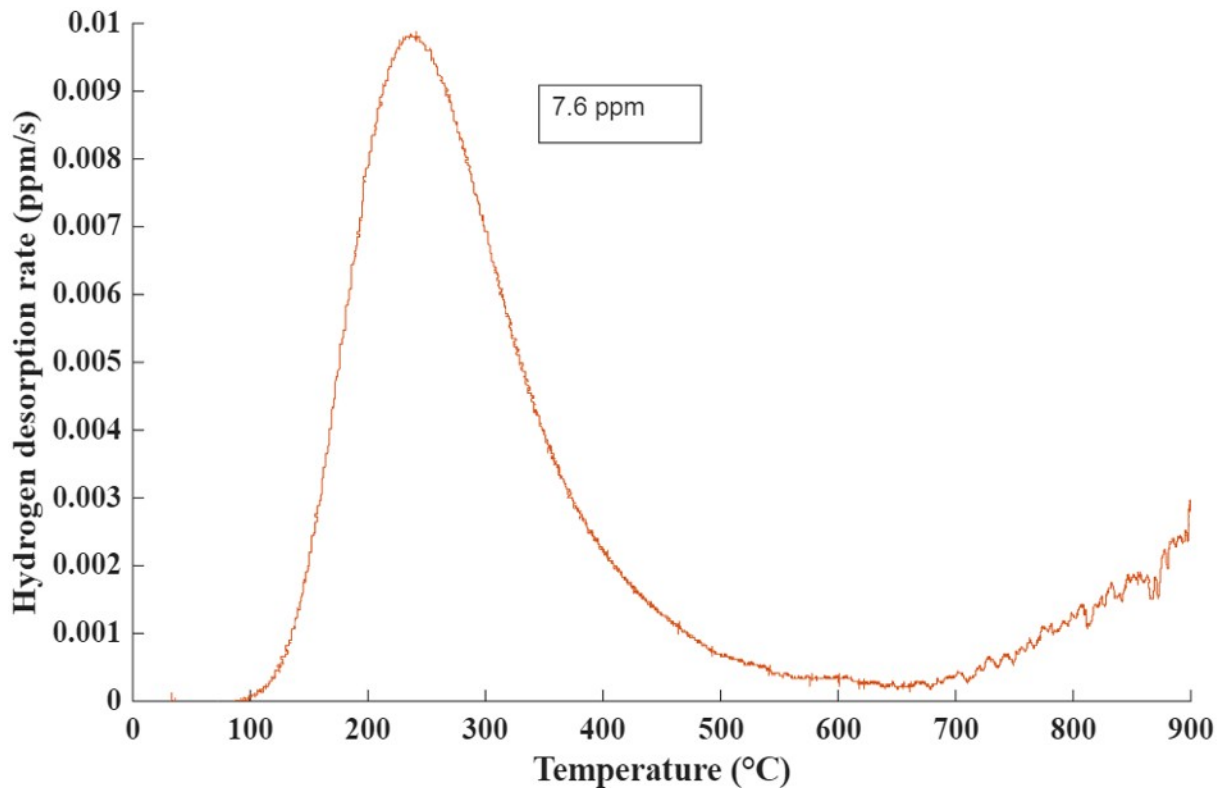


Figure 0.9: TDA desorption curve of DSS as temperature rises

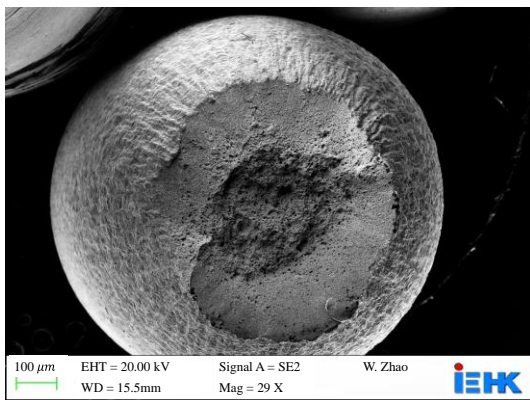
As the temperature increased, the amount of hydrogen released from the steel also increased, showing clear peaks at certain temperature ranges. At lower temperature, the hydrogen was trapped in weaker sites such as small defects, dislocations, or grain boundaries. These traps can release hydrogen easily. At higher temperatures show hydrogen coming out from stronger traps such as phase boundaries between ferrite and austenite. These traps hold hydrogen more tightly. The extreme part of the curve shows that hydrogen still comes out at very high temperatures, this means some hydrogen is still trapped in the material.

This explains that hydrogen in weak traps will leave quickly, but hydrogen in strong traps can stay for a long time causing the steel more likely to crack over time most especially in hydrogen rich environments.

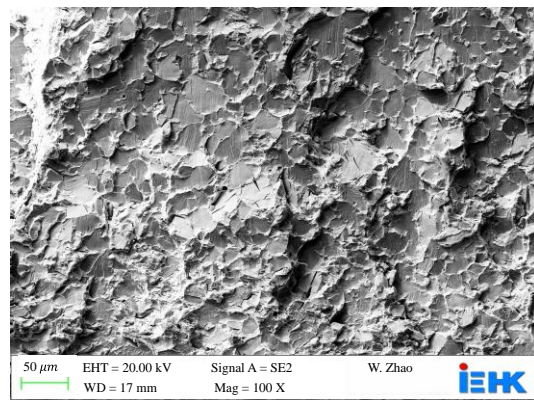
These peaks line up with different trap locations including dislocations, grain boundaries, and phase interfaces. According to the result, it shows that hydrogen is retained in both shallow and deep traps.

### **3.5 Fractographic Observation**

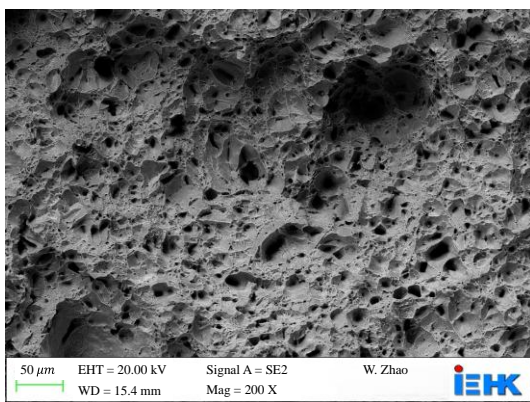
Fracture surface analysis was carried out using SEM, in order to understand the failure mechanisms under both air and hydrogen charged conditions. As shown in Figure 0.10, without hydrogen charging, SEM revealed ductile fracture features, including uniformly distributed dimples, indicative of microvoid coalescence typical of ductile tearing. Then under Hydrogen Charging, SEM shows brittle fracture features, such as the flat, shiny surfaces representing the cleavage facets; cracks running along the edges of grains representing the intergranular cracks and smaller cracks branching off from the main one which is the secondary cracks. All these indicates that the presence of hydrogen caused the material to shift from a tough, ductile way of breaking to a more sudden and brittle type of fracture.



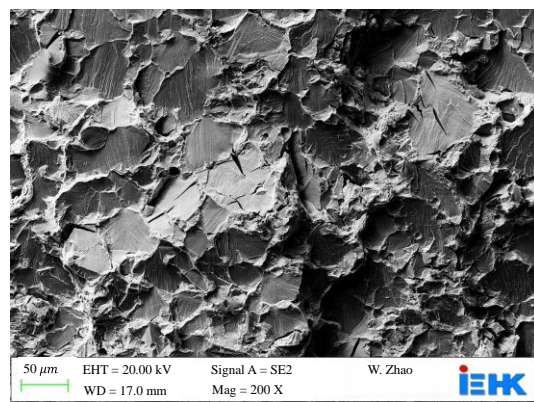
a.



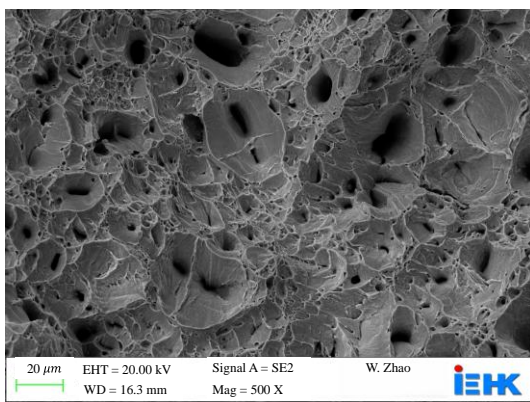
d.



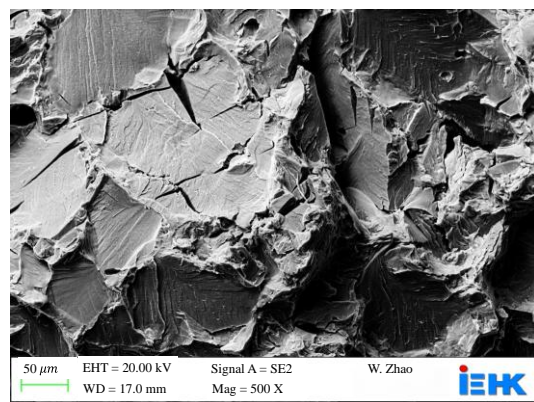
b.



e.



c.



f.

Figure 0.10: Figures a, b and c indicate the In Air SEM imagery while Figures d, e and f indicates under Hydrogen Charging SEM imagery.

Table 0.2: SEM Image Parameters

Parameters	Meaning
Scale bar in $\mu\text{m}$	This shows the actual length represented by the bar in the image (green coloured). To be able to estimate the size of features.
EHT in kV	Electron high tension is the accelerating voltage applied to the beam of the electron. The beam has high energy, which allows it to penetrate deeper into the provided sample for better resolution.
WD	Working distance is the distance between the sample surface and the lens of the electron. This gives more depth of field.
Signal A = SE2	Type of detector used. SE2 means secondary electrons type 2, gives topographical information that is surface features for viewing fractured surfaces or rough textures.
Mag	Magnification, this shows image larger than the actual size.

### 3.6 Discussion

Figures 3.11 and 3.12 illustrate the tensile behaviour under simultaneous electrochemical hydrogen charging. It was noticed that there is a quick drop in both the ultimate tensile strength and also the elongation compared to the In-air sample.

The curve shows a premature failure, this shows that hydrogen charging causes embrittlement, thereby reducing its ductility and strength. Therefore, one can say that the introduction of hydrogen helps weakens the bonds thereby accelerating its failure. This confirms the previous reports on DSS made by Francis and Byrne (Francis and Byrne, 2021) under hydrogen assisted cracking.

The degradation in mechanical performance shows the hydrogen embrittlement vulnerability of DSS.

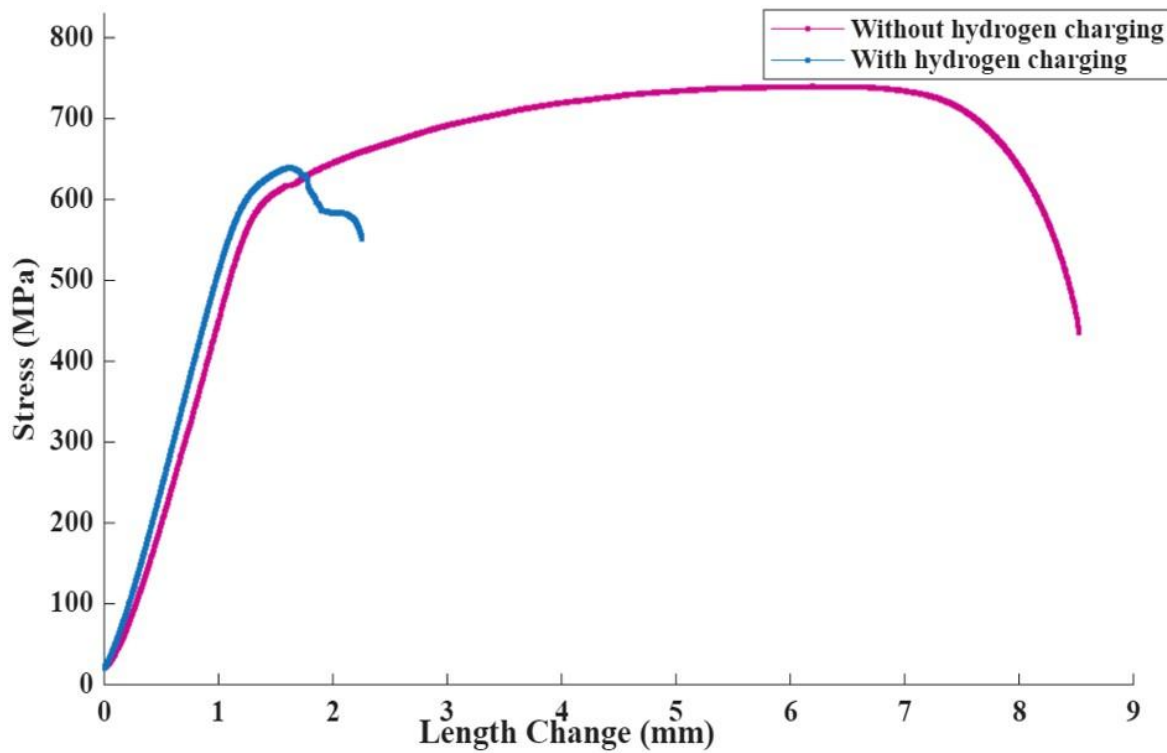


Figure 0.11: Combined stress-length change curves

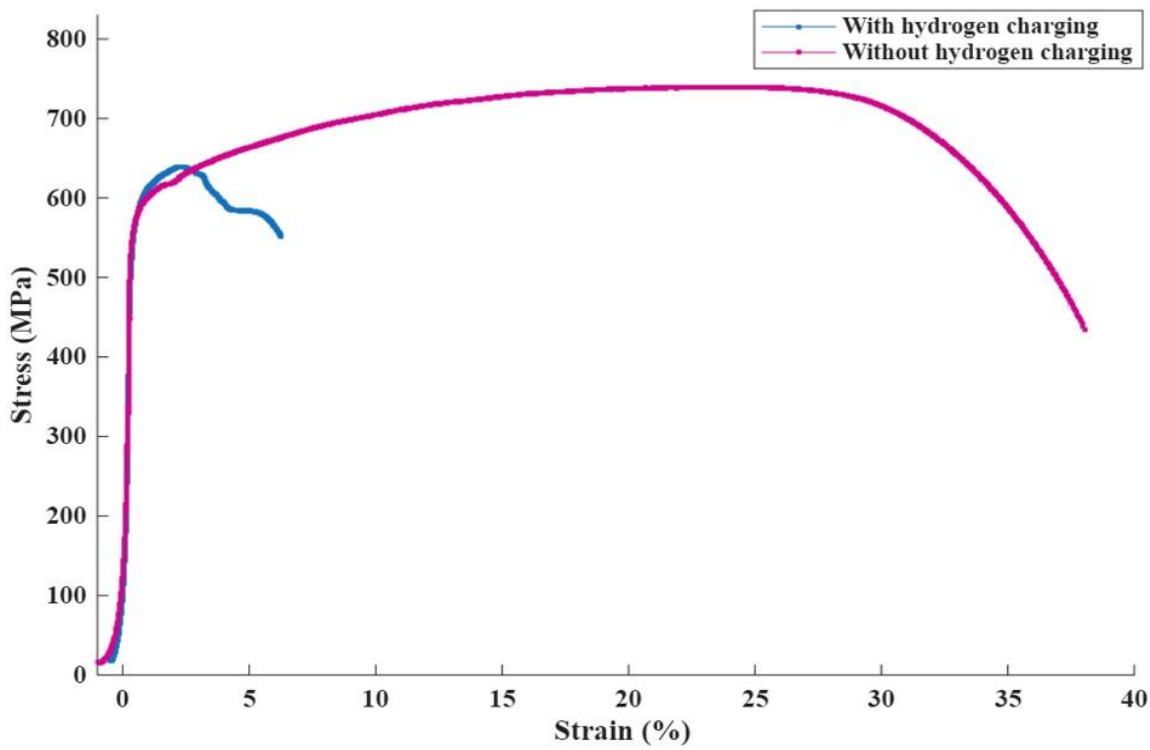


Figure 0.12: Combined stress-strain curves

Table 0.3: Mechanical comparison In-Air versus hydrogen charged

Parameters	In-Air	With Hydrogen Charging
Yield Strength (MPa)	576	579
Ultimate tensile Strength (MPa)	740	639
Uniform Elongation (%)	23	2
Total elongation (elongation at fracture) (%)	38	6
Time to Failure (s)	64113 (17.8 hrs)	17079 (4.7 hrs)

Comparing how the duplex stainless steel (DSS) performed in normal air and under hydrogen exposure during testing.

Looking at the yield strength (MPa), that is the stress at which the material starts to deform permanently, we can see that is almost the same in both cases. We can say that hydrogen did not significantly affect the point where the steel starts to yield at least at strain rate of  $5 \cdot 10^{-6}$ .

The ultimate tensile strength (UTS, MPa), under hydrogen charging, the maximum stress the material could withstand before breaking dropped sharply. With a 14% drop in peak strength at the presence of hydrogen. This shows that while the steel started off strong, hydrogen quickly reduced its ability to carry load at the highest stress levels. This means that hydrogen made the steel weaker at its peak load capacity. This observation agrees with earlier work of (Knyazeva and Pohl, 2013), also observing a significant embrittlement of DSS when exposed to hydrogen rich environments.

At the Uniform elongation, the steel stretched evenly much less under hydrogen, a huge drop from 23% to 2%. This indicates that hydrogen made the steel lose the majority of its capacity to deform uniformly before necking, it shows a strong embrittlement effect.

The total elongation at fracture shows the overall stretch before breaking reduced by about 84%, this means that the steel became far less ductile in hydrogen environments.

The time of failure(s), here the steel lasted much shorter under hydrogen charging before failure, this means that hydrogen sped up the failure process, even at slow strain rates.

Hydrogen charging did not change when yielding started but resulted to a big decrease in maximum tensile strength, a huge loss in ductility (both uniform and total elongation) and a shorter service life under loading. This shows hydrogen embrittlement, where the fracture mode changes from ductile and brittle, making the material unsafe in hydrogen rich conditions without proper mitigation.

Generally, the chemical composition given and the heat treatment produced a well-balanced duplex microstructure that is ideal for both strength and corrosion resistance. This shows that after heat treatment the duplex stainless steel (DSS) retains the dual phase advantages, the high

strength provided by ferrite and the corrosion resistance offered by austenite.

During the in-situ hydrogen charging in slow strain rate test (SSRT), there was clearly a drop in the tensile performance and ductility, indicating hydrogen embrittlement. This effect limits the safe use of DSS in hydrogen pipelines, and fuel cell systems unless additional protective measures, such as surface coatings or chemical inhibitors are used.

Thermal desorption analysis shows that hydrogen was absorbed and retained in the steel, especially in trap sites located along ferrite boundaries and dislocations. The presence of these traps might assist in delaying failure even after the hydrogen source is removed, although they may also serve as possible initiation sites for cracking over time.

Fractography examination revealed a transition from ductile to brittleness under the exposure of hydrogen, showing the hydrogen fundamentally changes the way the steel fractures.

Finally, it was discovered that the behaviour corresponds well with the already established hydrogen embrittlement mechanisms, these includes the hydrogen-enhanced decohesion (HEDE) and hydrogen-enhanced localized plasticity (HELP). By better understanding these mechanisms makes it possible to better predict and failure behaviours modelled, leading to better material selection and the development of effective prevention measures for critical hydrogen infrastructure.

### **3.7 Partial Conclusion**

- a. The metallography and the heat treated DSS at 1250°C displayed excellent phase balance and microstructural uniformity.
- b. Mechanical deterioration was seen when samples were examined under hydrogen charging, which confirms vulnerability to embrittlement.
- c. TDA results showed that hydrogen is absorbed and trapped, especially in austenite rich areas.
- d. Fractography confirmed a change in failure mechanisms due to hydrogen interaction on the sample.
- e. The combination of SSRT, TDA, and metallography provides a comprehensive knowledge of embrittlement behaviour in DSS.

# **GENERAL CONCLUSION AND PERSPECTIVE**

## GENERAL CONCLUSION

This study examines the microstructural characterization and hydrogen embrittlement behaviour of duplex stainless steels (DSS) by using a combination of slow strain rate testing (SSRT), in-situ SSRT under hydrogen charging, and thermal desorption analysis (TDA).

It was confirmed that the chosen type of duplex stainless steel, having a balanced austenite-ferrite microstructure, provides a strong combination of mechanical strength and corrosion resistance. However, when exposed to hydrogen environments, the steel experienced a significant deterioration in the mechanical properties such as the tensile performance and ductility, this clearly indicates the susceptibility to hydrogen embrittlement.

The experiments in this work were carried out under an ambient temperature ( $\sim 21$  °C). Under these conditions, the time of failure for the specimens that were tested in air was approximately 64,000 seconds, while under hydrogen charging failed much earlier after approximately 17,000 seconds. This drastic reduction shows the severity of hydrogen embrittlement, which accelerates failure even under mild test conditions.

Microstructural and fractography analysis further confirmed that a two-phases of duplex stainless steel respond differently in a hydrogen-rich environment. Ferrite shows to be more sensitive as it allowed rapid diffusion of hydrogen thereby promoting crack initiation and propagation while austenite on the other hand was less immediately affected. It acted as a trapping phase that stored hydrogen but resisted cracking for longer. For the crack initiation, the phase boundaries between ferrite and austenite were identified as the weakest regions, where there is stress concentration and non-uniform properties made them a suitable region.

Therefore, the findings confirm that duplex stainless steels, although strong and corrosion resistant, becomes highly vulnerable in hydrogen environments, thereby raising important considerations for its applications in the transportation of hydrogen, storage and in other related energy infrastructure, especially in the context of the emerging green hydrogen economy. To overcome these weaknesses, we need practical solutions such as protective coatings, improving the alloy's composition, and smarter design strategies such as designing an equipment to reduce stress concentrations by avoiding sharp corners and weak weld joints, or by adding thicker wall sections that provides extra margin of safety, also protective liners or claddings that act as a barrier against the ingress of hydrogen. These steps are important if duplex stainless steels are to be used safely and reliably in critical hydrogen applications.

## PERSPECTIVE

The insights I gained from this study open several perspectives for further research and industrial applications. The confirmation that DSS suffers significant embrittlement in hydrogen-rich environments shows the need to reanalyse its suitability for use in hydrogen related infrastructures such as hydrogen pipelines transport, storage vessels and fuel cell systems.

While duplex stainless steel remains attractive because of their combined strength and corrosion resistance, their vulnerability to hydrogen requires additional safeguards to ensure a long-term reliability and safety.

Further research should explore alloy modifications and heat-treatment optimization to improve resistance by achieving a stabilized phase balance as well as reducing weak interfaces where hydrogen-assisted cracking is most likely to occur. In addition, evaluation of protective surface treatments, coatings to make possible barriers to hydrogen ingress.

Industrially, these findings articulate the importance of developing material selection guidelines and predictive models that establishes hydrogen embrittlement in real conditions. This research is also relevant for the Africa's growing interest in the green hydrogen economy. As investments are directed towards hydrogen production, transportation and storage, the safe and cost-effective use of materials like DSS becomes critically important.

Therefore, the better understanding of HE and developing practical mitigation strategies will contribute immensely to the continent's ability to adopt green hydrogen technologies without hesitation.

Finally, the work provides a foundation of bridging the basic material science with practical engineering applications, to ensure that the transition to hydrogen-based energy systems is both safe and sustainable.

By taking care of these factors, the safe and sustainable use of duplex stainless steels in the evolving hydrogen economy can be more effectively achieved, which will guarantee both performance and dependability.

## REFERENCES

1. BSSA (2025), “Duplex Stainless Steels - A Simplified Guide”, available at: [https://bssa.org.uk/bssa\\_articles/2-duplex-stainless-steels-a-simplified-guide-2/](https://bssa.org.uk/bssa_articles/2-duplex-stainless-steels-a-simplified-guide-2/).
2. Catherine, Houska, C.S.I. (2015), “Duplex stainless steel revolutionizes structural design”.
3. Chen, M., Liu, S., He, K., Zheng, X., Zhang, Y., Tang, J. and Ye, L. (2023), “Hydrogen-induced failure in a partially-recrystallized Al-Zn-Mg-Cu alloy with different aging conditions: Influence of deformation behavior dominated by microstructures”, *Materials & Design*, Vol. 233, p. 112199.
4. Dwivedi, S.K. and Vishwakarma, M. ((2018)), “Hydrogen embrittlement in different materials: A review”, *International Journal of Hydrogen Energy*, Vol. 43 No. 46, pp. 21603–21616.
5. Fangnon, E., Malitckii, E., Yagodzinskyy, Y. and Vilaça, P. (2020), “Improved Accuracy of Thermal Desorption Spectroscopy by Specimen Cooling during Measurement of Hydrogen Concentration in a High-Strength Steel”, *Materials (Basel, Switzerland)*, Vol. 13 No. 5.
6. Francis, R. and Byrne, G. (2021), “Duplex Stainless Steels—Alloys for the 21st Century”, *Metals*, Vol. 11 No. 5, p. 836.
7. Fu, H., Wang, W., Zhao, H., Jin, F. and Li, J. (2020), “Study of hydrogen-induced delayed fracture in high-Mn TWIP/TRIP steels during in situ electrochemical hydrogen-charging: Role of microstructure and strain rate in crack initiation and propagation”, *Corrosion Science*, Vol. 162, p. 108191.
8. Gunn, N.R. (1997), *Duplex Stainless Steels: Microstructure, properties and applications*, 1st ed., Abington Publishing, Woodhead Publishing Ltd, Sawston, Cambridge, United Kingdom.
9. Han, J., Da Silva, A.K., Ponge, D., Raabe, D., Lee, S.-M., Lee, Y.-K., Lee, S.-I. and Hwang, B. (2017), “The effects of prior austenite grain boundaries and microstructural morphology on the impact toughness of intercritically annealed medium Mn steel”, *Acta Materialia*, Vol. 122, pp. 199–206.
10. Han, Y., Liu, Z.-H., Wu, C.-B., Zhao, Y., Zu, G.-Q., Zhu, W.-W. and Ran, X. (2023), “A short review on the role of alloying elements in duplex stainless steels”, *Tungsten*, Vol. 5 No. 4, pp. 419–439.
11. Henthorne, M. (2016), “The Slow Strain Rate Stress Corrosion Cracking Test—A 50 Year Retrospective”, *Corrosion*, Vol. 72 No. 12, pp. 1488–1518.

12. Klett, J. and T. Hassel (2020), “Reducing the risk of hydrogen-induced cold cracks in hyperbaric wet welding of high-strength steels by using austenitic welding consumables”, *Welding and Cutting*.
13. Knyazeva, M. and Pohl, M. (2013), “Duplex Steels: Part I: Genesis, Formation, Structure”, *Metallography, Microstructure, and Analysis*, Vol. 2 No. 2, pp. 113–121.
14. Li, J., Gao, X., Chen, H., Wu, H., Du, L. and Chen, C. (2023), “Hydrogen Embrittlement Susceptibility of Corrosion-Resistant Spring Rod Used in High-Speed Railway”, *Metals*, Vol. 13 No. 1, p. 147.
15. Liao, L. and Chumbley, S. (2019), “Influence of cooling rate on the ferrite content and microstructures in CD3MWCuN castings”, *SN Applied Sciences*, Vol. 1 No. 1.
16. Lynch, S.P. (2011), “Hydrogen embrittlement (HE) phenomena and mechanisms”, pp. 90–130.
17. Olanipekun, A.T., Nthabiseng, M., Ayodele, O.O., Mphahlele, M.R., Mampuya, B.M. and Olubambi, P.A. (2019), “Datasets on the measurement of mechanical properties of ferrite and austenite constitutive phases using nanoindentation and micro hardness techniques”, *Data in brief*, Vol. 27, p. 104551.
18. Pichler, S., Bendo, A., Mori, G., Safyari, M. and Moshtaghi, M. (2023), “Inhibition of grain growth by pearlite improves hydrogen embrittlement susceptibility of the ultra-low carbon ferritic steel: the influence of H-assisted crack initiation and propagation mechanisms”, *Journal of Materials Science*, Vol. 58 No. 33, pp. 13460–13475.
19. Rachel, P., Elin, M.W. and Mikael, J. (2013), “Corrosion performance of welds in duplex, superduplex and lean duplex stainless steels”, *Rivista Italiana della Saldatura*.
20. Tomoki, S. (2019), “Experimental Characterization of Influence of Gaseous Hydrogen on Fatigue Crack Propagation and Crack Tip Plasticity in Commercially Pure Iron”, Phd, Sciences et Ingénierie des Matériaux, Mécanique, Energétique, ISAE-ENSMA Ecole Nationale Supérieure de Mécanique et d’Aérotechique, Poitiers, France, 2019.

